J|A|C|S
ARTICLES

Published on Web 11/12/2008

Polyplexes from Poly(aspartamide) Bearing 1,2-Diaminoethane Side Chains Induce pH-Selective, Endosomal Membrane Destabilization with Amplified Transfection and Negligible Cytotoxicity

Kanjiro Miyata,[†,‡] Makoto Oba,[§] Masataka Nakanishi,[||] Shigeto Fukushima,[⊥] Yuichi Yamasaki,[||,‡] Hiroyuki Koyama,[§] Nobuhiro Nishiyama,[⊥,‡] and Kazunori Kataoka*[,†,||,⊥,‡]

Department of Bioengineering and Department of Materials Engineering, Graduate School of Engineering, and Center for NanoBio Integration, The University of Tokyo, 7-3-1 Hongo, Bunkyo-ku, Tokyo 113-8656, Japan, Department of Clinical Vascular Regeneration, Graduate School of Medicine, The University of Tokyo, 7-3-1 Hongo, Bunkyo-ku, Tokyo 113-8655, Japan, and Center for Disease Biology and Integrative Medicine, Graduate School of Medicine, The University of Tokyo, 7-3-1 Hongo, Bunkyo-ku, Tokyo 113-0033, Japan

Received June 23, 2008; E-mail: kataoka@bmw.t.u-tokyo.ac.jp

Abstract: Polyplexes assembled from poly(aspartamide) derivatives bearing 1,2-diaminoethane side chains, [PAsp(DET)] display amplified in vitro and in vivo transfection activity with minimal cytotoxicity. To elucidate the molecular mechanisms involved in this unique function of PAsp(DET) polyplexes, the physicochemical and biological properties of PAsp(DET) were thoroughly evaluated with a control bearing 1,3-diaminopropane side chains, PAsp(DPT). Between PAsp(DET) and PAsp(DPT) polyplexes, we observed negligible physicochemical differences in particle size and ζ-potential. However, the one methylene variation between 1,2-diaminoethane and 1,3-diaminopropane drastically altered the transfection profiles. In sharp contrast to the constantly high transfection efficacy of PAsp(DET) polyplexes, even in regions of excess polycation to plasmid DNA (pDNA) (high N/P ratio), PAsp(DPT) polyplexes showed a significant drop in the transfection efficacy at high N/P ratios due to the progressively increased cytotoxicity with N/P ratio. The high cytotoxicity of PAsp(DPT) was closely correlated to its strong destabilization effect on cellular membrane estimated by hemolysis, leakage assay of cytoplasmic enzyme (LDH assay), and confocal laser scanning microscopic observation. Interestingly, PAsp(DET) revealed minimal membrane destabilization at physiological pH, yet there was significant enhancement in the membrane destabilization at the acidic pH mimicking the late endosomal compartment (pH ~5). Apparently, the pH-selective membrane destabilization profile of PAsp(DET) corresponded to a protonation change in the flanking diamine unit, i.e., the monoprotonated gauche form at physiological pH and diprotonated anti form at acidic pH. These significant results suggest that the protonated charge state of 1,2-diaminoethane may play a substantial role in the endosomal disruption. Moreover, this novel approach for endosomal disruption neither perturbs the membranes of cytoplasmic vesicles nor organelles at physiological pH. Thus, PAsp(DET) polyplexes, residing in late endosomal or lysosomal states, smoothly exit into the cytoplasm for successful transfection without compromising cell viability.

Introduction

Successful transfection with polycation-based gene vectors (polyplexes) significantly depends on the chemical structure of the incorporated polycations.[1,2] Polyethylenimine (PEI) and its derivatives display protonation of amino groups over a wide pH range. Following polyplex formation, these well-known polycations exert a high transfection efficacy through endosomal escape supported by the proton sponge hypothesis.[3,4] However, there remains a great concern for the availability of PEI-based polyplexes in translational research, mainly due to their problematic toxicity.[5,6] Thus, the rational design of a polyplex system exhibiting clinically relevant gene expression with minimal toxicity remains an urgent complication for clinical

[†] Department of Bioengineering.
[‡] Center for NanoBio Integration.
[§] Department of Clinical Vascular Regeneration.
[||] Department of Materials Engineering.
[⊥] Center for Disease Biology and Integrative Medicine.

(1) Pack, D. W.; Hoffman, A. S.; Pun, S.; Stayton, P. S. *Nature Rev. Drug Discovery* **2005**, *4*, 581–593.
(2) Mastrobattista, E.; van der Aa, M. A. E. M.; Hennink, W. E.; Crommelin, D. J. A. *Nature Rev. Drug Discovery* **2006**, *5*, 115–121.
(3) Boussif, O.; Lezoualc'h, F.; Zanta, M. A.; Mergny, M. D.; Scherman, D.; Demeneix, B.; Behr, J. *Proc. Natl. Acad. Sci. U.S.A.* **1995**, *92*, 7297–7301.
(4) Neu, M.; Fischer, D.; Kissel, T. *J. Gene Med.* **2005**, *7*, 992–1009.
(5) Fischer, D.; Li, Y.; Ahlemeyer, B.; Krieglstein, J.; Kissel, T. *Biomaterials* **2003**, *24*, 1121–1131.
(6) Moghimi, S. M.; Symonds, P.; Murray, J. C.; Hunter, A. C.; Debska, G.; Szewczyk, A. *Mol. Ther.* **2005**, *11*, 990–995.

10.1021/ja804561g CCC: $40.75

extension of nonviral gene vectors. To overcome polycationic toxicity, a promising strategy is the incorporation of hydrophilic and nonionic poly(ethylene glycol) (PEG) to shield the deleterious, excess cationic charge associated with these carriers. Indeed, PEGylated polyplexes (polyplex micelles) formed through the association of PEG−polycation copolymers with DNA[7−12] were biocompatible under in vivo conditions, leading to appreciable in vivo gene expression with lower toxic effects.[13−16]

Nevertheless, further improvements in polyplex micelle systems are needed to show higher transfection efficacy and lower cytotoxicity for clinical translation. This recurring and pervasive problem endures, thereby motivating studies devoted to modulate the micellar, polycationic structure for effective clinical application in human gene therapy. Recently, we found that a flanking benzyl ester group of PEG-*b*-poly(β-benzyl L-aspartate) (PBLA) underwent a quantitative aminolysis reaction with a variety of amine compounds under a very mild condition,[17] allowing us to prepare an N-substituted poly(aspartamide) (PAsp) derivative library possessing a variety of cationic side chains from a single platformed PBLA.[18−25] A series of transfection and cytotoxicity assays of polyplexes prepared from the N-substituted PAsp derivative library revealed a highly promising candidate, PEG-*b*-poly{*N*-[*N*-(2-aminoethyl)-2-aminoethyl]aspartamide} (PEG−PAsp(DET)). A 1,2-diaminoethane unit was introduced as a side chain into PEG-*b*-PAsp, forming PEG-*b*-PAsp(DET); a series of primary cells and cultured cell lines were transfected, and significant gene expression with limited cytotoxicity was obtained. PEG−*b*-PAsp(DET) displayed high transfection efficacy comparable to commercially available linear PEI (ExGen 500) and the lipid-based system (Lipofectamine 2000); moreover, cytotoxicity levels were substantially lower compared to the controls.[15,16,19,21−25] Furthermore, PEG−PAsp(DET) polyplex micelles were successfully transfected in two animal models: (i) a rabbit's clamped carotid artery with neointima via intra-arterial injection[15] and (ii) a mouse skull by regulated release from a calcium phosphate cement scaffold to induce bone regeneration through the differentiation factor transduction.[16] The success of PEG−PAsp(DET) gene delivery in vivo has been attributed to the unique 1,2-diaminoethane structure in the side chain, where the *N*-(2-aminoethyl)-2-aminoethyl group exhibits a distinctive two-step protonation behavior. This dual protonation state suggests a strong pH-buffering capacity of Asp(DET) units for efficient endosomal escape.[19,21] Nevertheless, it still remains unknown whether the protonation behavior provides the crucial factor for excellent transfection when incorporated with PEG−PAsp. In parallel, it is unclear whether the low cytotoxicity of PEG−PAsp(DET) polyplex micelles is related to the particular cationic structure of Asp(DET) or simply due to the biocompatible PEG outer layer of the polyplex micelles.

These issues motivated us to clarify the structural factor of PAsp(DET) on transfection efficacy as well as cytocompatibility for additional polycationic structures successful for human gene therapy. To properly address the many architectural and chemical contributions of PEG−PAsp(DET), the following poly(aspartamides) were employed: (i) PAsp(DET) homopolymers to elucidate the effect of Asp(DET) units without PEGylation and (ii) a poly(aspartamide) bearing 1,3-diaminopropane units in the side chain as a control for 1,2-diaminoethane units, poly{*N*-[*N*-(3-aminopropyl)-3-aminopropyl]aspartamide} [PAsp(DPT)]. PAsp(DPT) exhibited a protonation degree over 88% at physiological pH and was considered to have a weak proton sponge effect. The high protonated state of Asp(DPT) at physiological pH is explained by the lowered electrostatic repulsion between the protonated diamine side chain units by the additional methylene group compared to Asp(DET). Detailed analysis of cellular membrane destabilization by PAsp(DET) and PAsp(DPT) revealed the distinct behavior of PAsp(DET) to facilitate membrane destabilization at the acidic pH of late endosomal or lysosomal states. This pH-selective membrane destabilization allows endosomal escape of PAsp(DET) polyplexes into the cytoplasm with limited toxicity to the other cytoplasmic membranes lying at neutral pH.

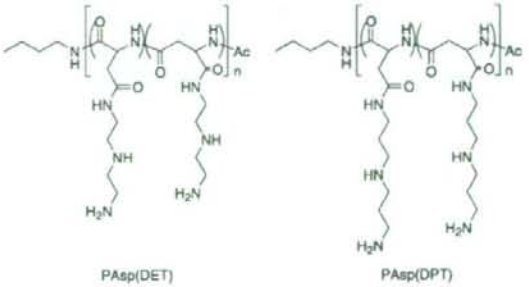

Results and Discussion

Protonation Degree (α) and Apparent pK_a of PAsp(DET) and PAsp(DPT). Previous studies revealed that a high transfection efficacy of PEI-based polyplexes was ascribed to their efficient endosomal escape, possibly due to the increased

(7) Kakizawa, Y.; Kataoka, K. *Adv. Drug Delivery Rev.* **2002**, *54*, 203–222.
(8) Katayose, S.; Kataoka, K. *Bioconjugate Chem.* **1997**, *8*, 702–707.
(9) Wolfert, M. A.; Schacht, E. H.; Toncheva, V.; Ulbrich, K.; Nazarova, O.; Seymour, L. W. *Human Gene Ther.* **1996**, *10*, 2123–2133.
(10) Choi, Y. H.; Liu, F.; Kim, J.; Choi, Y. K.; Park, J. S.; Kim, S. W. *J. Controlled Release* **1998**, *54*, 39–48.
(11) Vinogradov, S. V.; Bronich, T. K.; Kabanov, A. V. *Bioconjugate Chem.* **1998**, *9*, 805–812.
(12) Blessing, T.; Kursa, M.; Holzhauser, R.; Kircheis, R.; Wagner, E. *Bioconjugate Chem.* **2001**, *12*, 529–537.
(13) Harada-Shiba, M.; Yamauchi, K.; Harada, A.; Takamisawa, I.; Shimokado, K.; Kataoka, K. *Gene Ther.* **2002**, *9*, 407–414.
(14) Miyata, K.; Kakizawa, Y.; Nishiyama, N.; Yamasaki, Y.; Watanabe, T.; Kohara, M.; Kataoka, K. *J. Controlled Release* **2005**, *109*, 15–23.
(15) Akagi, D.; Oba, M.; Koyama, H.; Nishiyama, N.; Fukushima, S.; Miyata, T.; Nagawa, H.; Kataoka, K. *Gene Ther.* **2007**, *14*, 1029–1038.
(16) Itaka, K.; Ohba, S.; Miyata, K.; Kawaguchi, H.; Nakamura, K.; Takato, T.; Chung, U.; Kataoka, K. *Mol. Ther.* **2007**, *15*, 1655–1662.
(17) Nakanishi, M.; Park, J.-S.; Jang, W.-D.; Oba, M.; Kataoka, K. *React. Funct. Polym.* **2007**, *67*, 1361–1372.
(18) Fukushima, S.; Miyata, K.; Nishiyama, N.; Kanayama, N.; Yamasaki, Y.; Kataoka, K. *J. Am. Chem. Soc.* **2005**, *127*, 2810–2811.
(19) Kanayama, N.; Fukushima, S.; Nishiyama, N.; Itaka, K.; Jang, W.-D.; Miyata, K.; Yamasaki, Y.; Chung, U.; Kataoka, K. *ChemMedChem.* **2006**, *1*, 439–444.
(20) Arnida,; Nishiyama, N.; Kanayama, N.; Jang, W.-D.; Yamasaki, Y.; Kataoka, K. *J. Controlled Release* **2006**, *115*, 208–215.
(21) Han, M.; Bae, Y.; Nishiyama, N.; Miyata, K.; Oba, M.; Kataoka, K. *J. Controlled Release* **2007**, *121*, 38–48.
(22) Miyata, K.; Fukushima, S.; Nishiyama, N.; Yamasaki, Y.; Kataoka, K. *J. Controlled Release* **2007**, *122*, 252–260.
(23) Masago, K.; Itaka, K.; Nishiyama, N.; Chung, U.; Kataoka, K. *Biomaterials* **2008**, *28*, 5169–5175.
(24) Takae, S.; Miyata, K.; Oba, M.; Ishii, T.; Nishiyama, N.; Itaka, K.; Yamasaki, Y.; Koyama, H.; Kataoka, K. *J. Am. Chem. Soc.* **2008**, *130*, 6001–6009.
(25) Lee, Y.; Miyata, K.; Oba, M.; Ishii, T.; Fukushima, S.; Han, M.; Koyama, H.; Nishiyama, N.; Kataoka, K. *Angew. Chem., Int. Ed.* **2008**, *47*, 5163–5166.

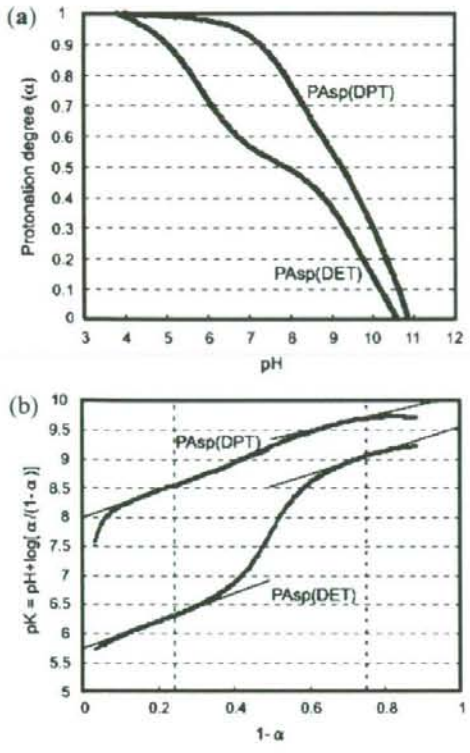

Figure 1. Protonation behavior of PAsp(DET) and PAsp(DPT). (a) Change in protonation degree (α) with pH (α/pH curve) (150 mM NaCl, 37 °C). (b) Change in apparent pK with $1 - \alpha$ [pK/$(1 - \alpha)$ curve].

osmotic pressure caused by facilitated protonation of polycations in endosomal acidic compartments (the proton sponge effect).[3,4] Hence, the difference in the protonation degree between neutral pH and endosomal acidic pH (from 7.4 to 5.0) has been considered to be a crucial factor for successful transfection with polycation-based systems. In this regard, the α of PAsp(DET) and PAsp(DPT) was estimated from the potentiometric titration, which was monitored over the range of pH 2.3−12 in the 150 mM NaCl solution at 37 °C, mimicking the physiological condition. As shown in Figure 1a, the α/pH curves calculated from the obtained titration curves (data not shown) revealed that the protonation behavior of the cationic poly(aspartamides) fairly depended on the number of methylene groups between the primary and secondary amino groups in the side chain. PAsp(DET) exhibited a substantial change in the α from neutral pH 7.4 to acidic pH 5.0 due to a distinctive two-step protonation behavior; i.e., 37% increase in the α through the pH drop from 7.4 to 5.0. In contrast, PAsp(DPT) showed facilitated protonation typically at physiological pH, and consequently, the increase in the α by changing pH from 7.4 to 5.0 was only 10%, an approximately 4 times smaller value than that expected for PAsp(DET). These results indicate that PAsp(DET) has potentially higher buffering capacity in endosomal acidic compartments than PAsp(DPT).

From the distinctive two-step protonation behavior of PAsp(DET), it is reasonably concluded that the first and the second protonation in the side chain proceeds separately. The remarkable difference in the protonation behavior between PAsp(DET)

Scheme 1. Two-Step Protonation of the 1,2-Diaminoethane Moiety in the Side Chain of PAsp(DET)

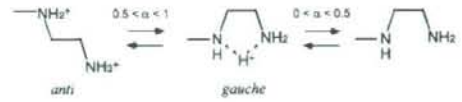

and PAsp(DPT) in the region of $0.5 < \alpha < 1$ indicates that the 1,2-diaminoethane unit in PAsp(DET) has restricted second protonation compared to the 1,3-diaminopropane unit in PAsp(DPT). The pK (=pH + log[α/(1 − α)]) values of PAsp(DET) and PAsp(DPT) were then calculated and plotted against $1 - \alpha$. Figure 1b clearly displays that PAsp(DET) has a substantially lower pK value in the range of $0 < 1 - \alpha < 0.5$, corresponding to the second protonation, than PAsp(DPT). Herein, apparent pK_a values in the first and the second protonations were defined as pK_{a1} ($\alpha = 0.25$) and pK_{a2} ($\alpha = 0.75$), respectively, and eventually were determined as follows: p$K_{a1,DET} = 9.1$ and p$K_{a2,DET} = 6.3$ for PAsp(DET), and p$K_{a1,DPT} = 9.7$ and p$K_{a2,DPT} = 8.6$ for PAsp(DPT). Although a large difference was not observed for K_{a1}, 2 orders of magnitude difference was observed for K_{a2}. It is worth noting that p$K_{a2,DET}$ was much lower than p$K_{a1,DET}$, indicating that the diprotonated form of the PAsp(DET) side chain suffers a thermodynamic penalty, presumably due to the electrostatic repulsion between two charged amino groups in the 1,2-diaminoethane moiety. The available conformation may be limited to an anti form according to three-bond interaction, i.e., butane effect, as shown in Scheme 1 to minimize the steric as well as electrostatic repulsion. As a result, the 1,2-diaminoethane side chain in PAsp(DET) takes a monoprotonated form at physiological pH ($\alpha = 0.53$ at pH 7.4) as calculated from Figure 1a. Alternatively, addition of a single, hydrophobic methylene group in 1,3-diaminopropane units reduces the repulsion between the charged amino groups to increase the conformational freedom, leading to the smooth second protonation in PAsp(DPT) ($\alpha = 0.88$ at pH 7.4). Note that both the 1,2-diaminoethane and 1,3-diaminopropnae, in PAsp(DET) and PAsp(DPT), respectively, may prefer to take the gauche conformation at the monoprotonated state, which is supported from the molecular orbital calculation.[26,27]

Preparation and Characterization of Polyplexes from PAsp(DET) and PAsp(DPT). The polyplex formation of PAsp(DET) and PAsp(DPT) was confirmed by agarose gel electrophoresis. The free pDNA band disappeared at N/P = 2 and 1.5 for PAsp(DET) and PAsp(DPT), respectively, indicating that all the pDNA molecules were associated with the polycations in the electrophoregram (Supporting Figure 2, Supporting Information). To quantitatively evaluate the relationship between N/P ratio and pDNA complexation with cationic PAsp(DET) and PAsp(DPT), an EtBr exclusion assay was completed. In this assay, pDNA complexation prevents EtBr molecules from intercalating into pDNA, resulting in the decrease in the EtBr fluorescence. Indeed, the EtBr fluorescence decreased with the increase in N/P ratios (Figure 2a), indicating the progressive complexation of pDNA with the polycations forming polyplexes. Also, Figure 2a exhibits that the inflection points of the fluorescence intensity are at N/P = 2 for PAsp(DET) and 1.4 for PAsp(DPT). These inflection points are in good agreement

(26) Corte, D. D.; Schelapfer, C.-W.; Daul, C. *Theor. Chem. Acc.* **2000**, *105*, 39–45.
(27) Bouchoux, G.; Choret, N.; Berruyer-Penaud, F. *J. Phys. Chem. A* **2001**, *105*, 3989–3994.

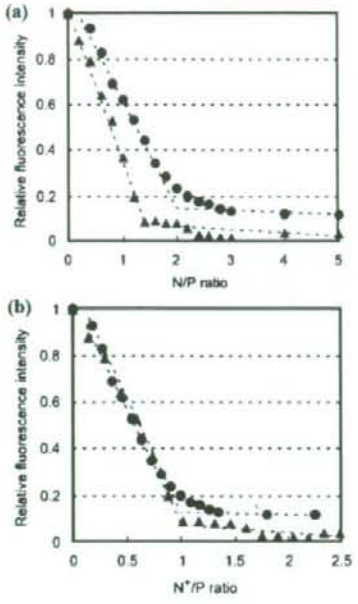

Figure 2. Ethidium bromide exclusion assay on PAsp(DET) and PAsp(DPT) polyplexes. (a) Relative fluorescence intensity vs N/P ratio. (b) Relative fluorescence intensity vs N^+/P ratio: (●) PAsp(DET) and (▲) PAsp(DPT).

with the N/P ratio where the free pDNA band disappeared from the electrophoregram (Supporting Figure 2, Supporting Information). These fluorescence data were replotted against N^+/P ratios, which were defined as the molar ratio of protonated amino groups at pH 7.4 in the polycations to phosphate groups in pDNA, as seen in Figure 2b. Note that the protonation degree of the amino groups of PAsp(DET) and PAsp(DPT) was determined to be 0.45 and 0.73 at pH 7.4, respectively, from the titration results without NaCl (data not shown). Obviously, both systems had the coincident inflection point of the fluorescence intensity at the N^+/P of unity, being consistent with the polyion-coupling between a phosphate group and an amino group in the protonated form expected from the α/pH curves. This result suggests that the pK_a value of PAsp(DET) shows minimal change with the polyplex formation, probably due to the thermodynamic penalty in diprotonated form of Asp(DET) units due to strong three-bond interaction (butane effect) caused by electrorepulsive interaction between two protonated amino groups.

The size and ζ-potential of polyplexes from PAsp(DET) and PAsp(DPT) in 10 mM Tris-HCl buffer (pH 7.4) were measured at 37 °C. As shown in Figure 3a, each polyplex had the critical range in N/P ratios, e.g., 2.5−3.5 and 1.4−1.5 for PAsp(DET) and PAsp(DPT), respectively, to reveal an appreciably large size of approximately 1000 nm. Considering that the ζ-potential of each polyplex was close to neutral in this critical range of N/P ratios, as seen in Figure 3b, these large-sized polyplexes may form through the secondary aggregation of the charge stoichiometric polyplexes showing minimal force of electrostatic repulsion. In the range over these critical N/P ratios, the size of both polyplexes were maintained <100 nm. The polyplexes in this range exhibited almost constant positive ζ-potential values (+30 mV) in both systems.

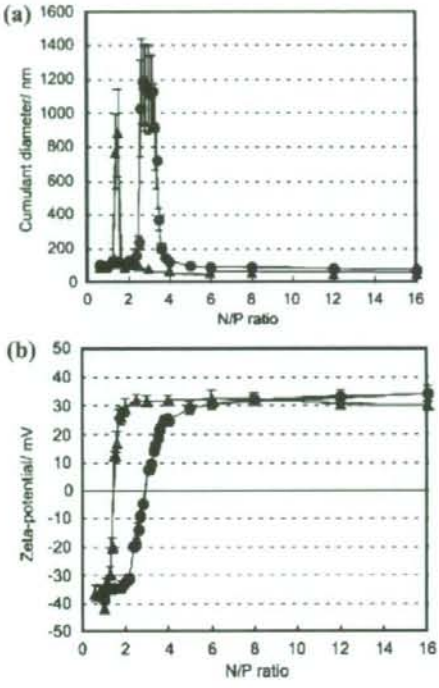

Figure 3. Change in the size and the ζ-potential of PAsp(DET) and PAsp(DPT) polyplexes with N/P ratio. (a) Cumulant diameter and (b) ζ-potential: (●) PAsp(DET), (▲) PAsp(DPT). All the samples were normalized to a concentration of 33 μg pDNA/mL at 37 °C. Results were expressed as mean ± SEM (n = 3).

Transfection Efficacy and Cytotoxicity of PAsp(DET) and PAsp(DPT) Polyplexes. The transfection efficacy of the luciferase gene against a human hepatocyte cell line (Huh-7) and a human umbilical vein endothelial cell (HUVEC) was compared between PAsp(DET) and PAsp(DPT) polyplexes. The polyplexes prepared at N/P ratios of 4, 8, and 16 were examined in this assay, having almost the same size and ζ-potential (Figure 3a,b). Polyplexes prepared from branched polyethylenimine (BPEI) (25 kDa) were used as a control. As seen in Figure 4a,b, the highest transfection efficacy in both cells was achieved by the PAsp(DET) polyplexes prepared at the N/P ratio of 16. This transfection efficacy of PAsp(DET) polyplexes was 1 order of magnitude higher than that of BPEI polyplexes against HUVEC. Obviously, the transfection efficacy of PAsp(DET) polyplexes was enhanced with the increase in N/P ratio against both cells. On the contrary, PAsp(DPT) exhibited the decrease in the transfection efficacy with the increase in N/P ratio. Considering that the large difference was not observed in the size and ζ-potential between PAsp(DET) and PAsp(DPT) polyplexes (Figure 3a,b), this opposite trend in transfection profiles of these two polyplexes against N/P ratio is likely to be due to the distinctive physicochemical properties directly related to the difference in the chemical structures, particularly the side chain structures. Interestingly, in the region of low N/P ratio, the PAsp(DPT) polyplexes revealed a comparable transfection efficacy to PAsp(DET) polyplexes, even though the former was expected to exert substantially weaker buffering capacity than the latter, as judged from the α/pH curve (Figure 1a).

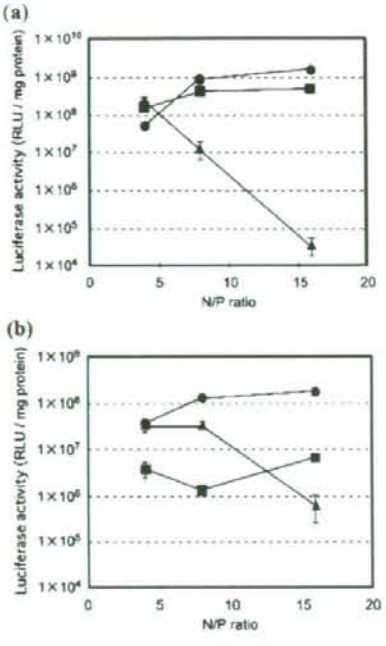

Figure 4. In vitro transfection of Huh-7 (a) and HUVEC (b) with PAsp(DET), PAsp(DPT), and BPEI polyplexes at varying N/P ratios evaluated by luciferase assays: (●) PAsp(DET), (▲) PAsp(DPT), and (■) BPEI. Results were expressed as mean ± SEM ($n = 4$).

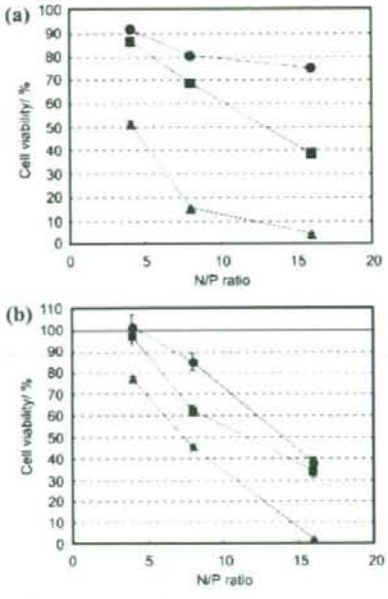

Figure 5. MTT cytotoxicity of Huh-7 (a) and HUVEC (b) with PAsp(DET), PAsp(DPT), and BPEI polyplexes evaluated under the same experimental conditions as in Figure 4 (luciferase assay): (●) PAsp(DET), (▲) PAsp-(DPT), and (■) BPEI. Results were expressed as mean ± SEM ($n = 4$).

There are several key steps in the transfection process of an exogenous gene, such as cellular uptake, intracellular trafficking, release of the gene from the complexes, transcription, and translation. Furthermore, excess polycationic charge with polyplexes is an issue to induce impaired cellular homeostasis, resulting in the negative influences on whole transfection steps, especially transcription and translation. Indeed, our previous study revealed that the challenge of linear PEI polyplexes into Huh-7 cells stably expressing firefly luciferase highly impaired the transcription and translation processes to reduce the expression of firefly luciferase as well as a variety of house-keeping genes.[2,3] In this regard, a toxicological assay was completed to explore the different transfection profiles between PAsp(DET) and PAsp(DPT) polyplexes against N/P ratio. As shown in Figure 5a,b, the results of the MTT cell viability assay, the cytotoxicity of each polyplex under the same experimental condition as the luciferase assay increased with N/P ratio for both cells, Huh-7 and HUVEC. This result is in good agreement with the result from the MTT assay of each polymer without pDNA (Supporting Figure 3a,b and Supporting Table 1, Supporting Information). Obviously, the PAsp(DET) polyplex had much lower toxicity than the PAsp(DPT) polyplex. In detail, at a N/P ratio of 16 in Huh-7 cells, the viability of cells incubated with PAsp(DET) polyplexes was over 70% of that of control cells, whereas the viability was less than 10% in the case of PAsp(DPT) polyplexes (Figure 5a). Similarly, the cytotoxicity of PAsp(DPT) polyplexes was the highest against HUVEC, followed by BPEI and PAsp(DET) polyplexes (Figure 5b). From these results, it is worth noting that only one additional methylene group between two amino groups in the side chain crucially elevates the cytotoxicity of the cationic poly(aspartamides). This high cytotoxicity of PAsp(DPT) might contribute to the dramatically decreased transfection efficacy of PAsp(DPT) polyplexes at high N/P ratios. In contrast, cytotoxicity was substantially lowered in PAsp(DET) polyplexes, allowing high transfection efficacy with the increased N/P ratio.

To explore the endosomal escaping behavior of PAsp(DET) and PAsp(DPT) polyplexes, HUVEC trafficking studies were completed with a confocal laser scanning microscope (CLSM). In this experiment, pDNA was labeled by Cy5 (red), and nucleus and late-endosome/lysosome were stained by Hoechst 33342 (blue) and LysoTracker (green), respectively. Figure 6a,e shows the intracellular distribution of BPEI polyplexes 3 and 12 h after administration, respectively, as a positive control exerting an endosomal escaping function. Obviously, the red regions surrounding the yellow regions, where Cy5-labeled pDNA was localized in late-endosomes or lysosomes, were widely observed over time. It may be reasonable to judge that these spreading red regions represent the distribution of polyplexes exiting from the late endosomal or lysosomal stage into the cytoplasm. On the contrary, the negative control, PLys polyplexes, which lack significant buffering capacity, displayed much less red regions (Figure 6d,h), suggesting the segregation of Cy5-labeled pDNA in endo/lysosomal compartments without diffusing into cytoplasm. The confocal images of the cells transfected by PAsp-(DET) polyplexes (Figure 6b,f) display spreading red regions into the cytoplasm, comparable to the previously described BPEI transfection. These data indicate facilitated transport of Cy5-labeled pDNA into the cytoplasm from the endo/lysosomal compartments. The CLSM images of PAsp(DET) polyplexes are consistent with the high buffering capacity of the native polymer. Interestingly, similar diffusing red regions were also observed for PAsp(DPT) polyplexes (Figure 6c,g), suggesting that PAsp(DPT) may facilitate endosomal escape of the polyplex, despite the previously determined poor pH-buffering capacity of PAsp(DPT). Indeed, PAsp(DPT) polyplexes showed

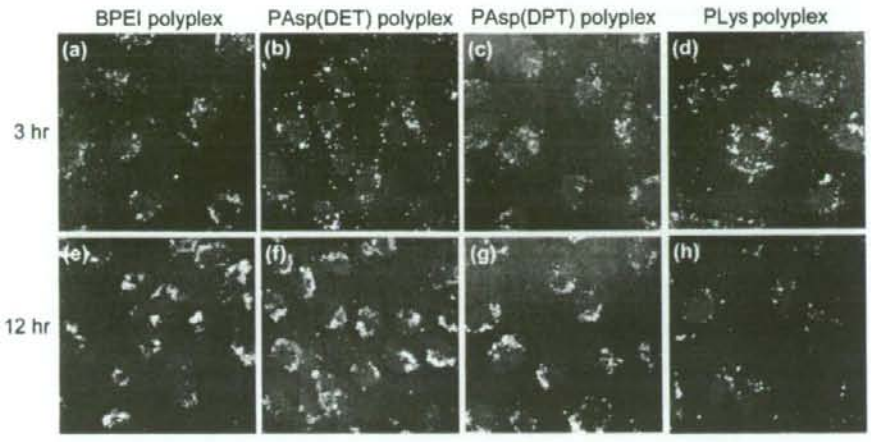

Figure 6. Intracellular distribution of Cy5-labeled pDNA complexed with a variety of polycations in HUVEC. Cy5-labeled pDNA and LysoTracker as a late-endosome and lysosome marker were observed in red and green, respectively. The cells were incubated at 37 °C for a definite time period, followed by washing with PBS, and subjected to CLSM imaging. Panels a–d and e–h are the images after 3 and 12 h incubation, respectively. (a and e) BPEI polyplexes (N/P = 8), (b and f) PAsp(DET) polyplexes (N/P = 8). (c and g) PAsp(DPT) polyplexes (N/P = 8). (d and h) PLys polyplexes (N/P = 2).

comparable transfection efficacy to BPEI and PAsp(DET) polyplexes at low N/P ratios (Figure 4a,b). These results strongly suggest the presence of another mechanism facilitating late endosomal or lysosomal escape beyond the putative proton sponge effect. Note that the medium change at 1 h after the polyplex administration significantly decreased the red regions (or dots) corresponding to endosomal escaping behavior in BPEI, PAsp(DET), and PAsp(DPT) (Supporting Figure 4, Supporting Information). This indicates that prolonged incubation of excess polyplexes with cells substantially facilitates the endosomal escape. Prolonged incubation should lead to the increased cellular uptake of polyplexes, presumably resulting in the polyplex accumulation with higher concentration in late-endosomal compartments to bring facilitated endosomal escape.

Membrane Destabilization by PAsp(DET) and PAsp(DPT). As described in the preceding section, the CLSM observation of Cy5-labeled pDNA in the intracellular compartment demonstrated that cytoplasmic transport efficiently occurred even for PAsp(DPT) polyplexes, known to possess the low buffering capacity. Of note, the previous studies addressed the destabilization of cellular membranes through the direct interaction with polycations,[5,6,28] possibly leading to the facilitated cytoplasmic transport of the polyplexes.[29–31] This destabilizing effect of polycations on the cellular membrane is considered to be dependent on the concentration (or N/P ratio), molecular weight, cationic charge density, and molecular structure of polycations.[5] Thus, the membrane destabilization induced by PAsp(DET) and PAsp(DPT) was estimated by the hemolysis assay, in which the amount of hemoglobin liberated from erythrocytes was determined from colorimetric analysis at 575 nm (Figure 7). Figure 7a clearly shows the significant difference in hemolytic activity between PAsp(DET) and PAsp(DPT) after an overnight incubation with murine erythrocytes at pH 7.4. The hemolytic activity of PAsp(DET) was negligible under the examined conditions, whereas PAsp(DPT) exhibited appreciable hemolytic activity in a concentration-dependent manner. Next, the hemolytic assays were repeated under acidic conditions indicative of the late endosomal or lysosomal state. Since overnight incubation of murine erythrocytes at pH 5.5 led to an appreciable decrease in the signal-to-noise ratio (Abs 575 nm), possibly due to instability of erythrocytes or conformational change of hemoglobins under the acidic condition, a shorter incubation time of 3 h was adopted. As clearly seen in Figure 7b, hemolytic activity levels were concentration-dependent for PAsp(DPT), regardless of the environmental pH. In direct contrast, however, the hemolytic activity of PAsp(DET) was critically enhanced by decreasing the environmental pH from 7.4 to 5.5 (Figure 7c), reaching the levels comparable to PAsp(DPT) (Figure 7b). The membrane destabilizing capacity of these polycations was further tested against HUVEC by a colorimetric LDH assay, in which the enzymatic activity of cytosolic LDH liberated from the cells was measured to estimate the membrane damages.[5,6] Figure 8a clearly shows that PAsp(DPT) induced LDH liberation in a concentration-dependent manner, both at acidic and physiological pH conditions. These data suggest a strong capacity of PAsp(DPT) to destabilize the endosomal membrane as well as the cytoplasmic membrane, regardless of the environmental pH. This is consistent with the results of the hemolysis assay shown in Figure 7b. Alternatively, the activity of LDH liberated from HUVEC incubated with PAsp(DET) was obviously low at pH 7.4, while the decrease in pH to acidic condition (pH ~5) substantially enhanced its activity to the same level as that of PAsp(DPT) (Figure 8b), exhibiting the similar trend to the hemolytic activity (Figure 7c). Similar results of the membrane destabilization were obtained for Huh-7 cells (data not shown). Apparently, the concentration-dependent increase in the membrane destabilization capacity of PAsp(DET) under the acidic condition corresponds to the enhanced transfection efficacy with N/P ratios (Figure 4).

We next sought to find a correlation between the interaction of the polycations with the membrane and the destabilization effect. CLSM observations were further carried out for HUVEC

(28) Zhang, Z.-Y.; Smith, B. D. *Bioconjugate Chem.* **2000**, *11*, 805–814.
(29) Merdan, T.; Kunath, K.; Fischer, D.; Kopecek, J.; Kissel, T. *Pharm. Res.* **2002**, *19*, 140–146.
(30) Bieber, T.; Meissner, W.; Kostin, S.; Niemann, A.; Elsasser, H.-P. *J. Controlled Release* **2002**, *82*, 441–454.
(31) Walker, G. F.; Fella, C.; Pelisek, J.; Fahrmeir, J.; Boeckle, S.; Ogris, M.; Wagner, E. *Mol. Ther.* **2005**, *11*, 418–425.

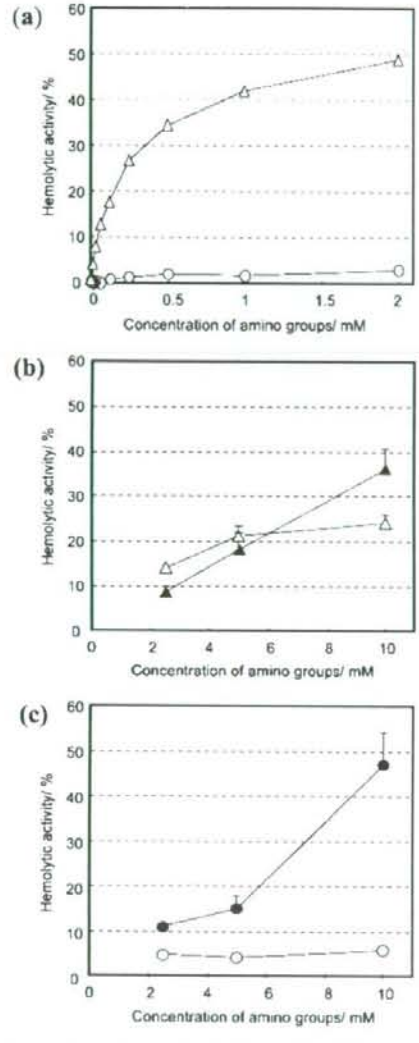

Figure 7. Hemolytic activity of PAsp(DET) and PAsp(DPT) against murine erythrocytes. (a) Hemolytic activity of PAsp(DET) (○) and PAsp(DPT) (△) after overnight erythrocyte incubation at pH 7.4 and 37 °C. (b) Hemolytic activity of PAsp(DPT) after 3 h incubation at pH 7.4 (△) and 5.5 (▲) (at 37 °C). (c) Hemolytic activity of PAsp(DET) after 3 h incubation at pH 7.4 (○) and 5.5 (●) (at 37 °C). Results were expressed as mean ± SEM ($n = 4$).

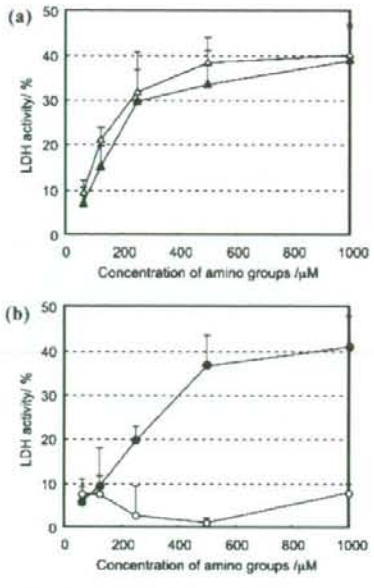

Figure 8. Enzymatic activity of LDH liberated from HUVEC upon interaction with the polycations at 37 °C for 1.5 h. (a) LDH activity for PAsp(DPT) system at pH 7.4 (△) and 5.5 (▲). (b) LDH activity for PAsp(DET) system at pH 7.4 (○) and 5.5 (●). Results were expressed as mean ± SEM ($n = 6$).

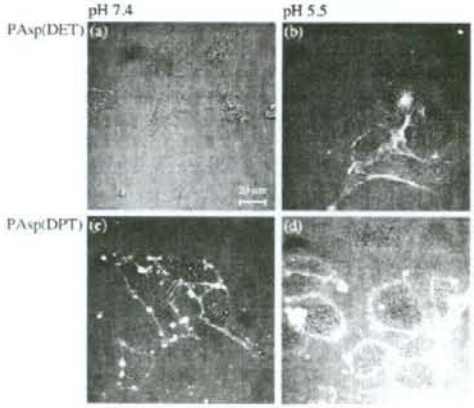

Figure 9. The adsorption of rhodamine B-labeled PAsp(DET) and PAsp(DPT) to HUVEC. The cells were incubated with the RhoB-labeled polycations (brightened as white) at the residual amino group concentration of 100 μM at 4 °C for 1 h, followed by washing with PBS, before CSLM imaging. (a) PAsp(DET) at pH 7.4, (b) PAsp(DET) at pH 5.5, (c) PAsp(DPT) at pH 7.4, (d) PAsp(DPT) at pH 5.5.

incubated with RhoB-labeled polycations. Fluorescence from PAsp(DET)−RhoB was not observed at pH 7.4 (Figure 9a) but upon acidic conditions (pH ~5), the fluorescence intensity was significant, extending to the cell periphery (Figure 9b), thereby indicating the appreciable cellular association of PAsp(DET)−RhoB at the acidic pH. In addition, CLSM studies with PAsp(DPT)−RhoB clearly showed significant levels of fluorescence at both pH's (Figure 9c,d), indicating a strong associative behavior of PAsp(DPT)−RhoB to cellular membrane, regardless of the pH. These images are in good agreement with the membrane-destabilizing capacity of the polycations determined by the hemolysis and LDH assays (Figures 7 and 8). It is reasonable to conclude from these results that PAsp(DPT), without high buffering capacity (Figure 1), facilitates endosomal escape of its polyplexes into the cytoplasm through the direct perturbation of endosomal membrane. Nevertheless, the strong capacity of membrane destabilization, even at physiological pH, induces substantial damage to the cell membrane treated with PAsp(DPT) polyplexes as confirmed by the poor cell viability (Figure 5a,b). On the contrary, the weak interaction of PAsp(DET) with the plasma membrane at neutral pH is consistent with the lowered membrane-destabilizing capacity indicated from the results of hemolysis and LDH

assays. These data are supported by the high viability of the cells treated with PAsp(DET) polyplexes, as judged by MTT assay (Figures 5a,b). It should be further emphasized that the cellular association and the membrane-destabilizing capacity of PAsp(DET) were significantly enhanced by decreasing environmental pH to 5.5, becoming comparable to those of PAsp(DPT). This indicates that PAsp(DET) selectively destabilizes the membrane of the endosomal compartment with decreased pH to facilitate the endosomal escape of the polyplexes with minimal damage to the plasma membrane facing an extracellular pH of 7.4. Furthermore, it is reasonable to assume that cytoplasmic PAsp(DET) polyplexes may show minimal interaction with the membranes of organelles because of the pH recovery from acidic to neutral accompanied by the migration from the endosome to cytoplasm. Eventually, PAsp(DET) polyplexes successfully achieved the high transfection efficacy without impairing the cellular viability, as seen in Figure 4.

The unique pH dependency of the affinity of PAsp(DET) to cellular membrane is apparently correlated with the two-step protonation behavior of the flanking 1,2-diaminoethane unit in PAsp(DET). As described in the former section, the 1,2-diaminoethane unit assumes a monoprotonated gauche form at neutral pH, while additional protonation at an acidic pH induces a conformational transition to a diprotonated anti form (Scheme 1). This protonation change accompanying the conformational transition is likely related with the pH-modulated interaction of PAsp(DET) with the cellular membrane. Apparently, PAsp(DET) with the diamine unit in the monoprotonated gauche state exhibited a weak affinity for the cellular membrane but the diprotonated anti state revealed an increased affinity to perturb the membrane integrity. In contrast, the 1,3-diaminopropane unit in PAsp(DPT) assumes a diprotonated form at physiological, late endosomal, and lysosomal pH conditions; moreover, PAsp(DPT) shows a strong interaction with the cellular membrane, even at neutral pH conditions.

Conclusion

The present study was devoted to clarify key chemical parameters for the next generation of polycation/polyplexes exhibiting augmented levels of transfection efficacy and negligible cytotoxicity both in vitro and in vivo. This work primarily focused on N-substituted cationic poly(aspartamide) derivatives, PAsp(DET), possessing flanking 1,2-diaminoethane side chain, previously identified for effective in vivo transfection.[15,16] Comparative analysis between PAsp(DET) and PAsp(DPT) revealed that a single methylene unit difference in the diamine side chains had a crucial effect on the multiple cationic charge states. This seemingly minimal chemical change produced a striking contrast in their polyplex transfection behaviors, presumably due to the increased cytotoxicity. The high cytotoxicity of PAsp(DPT) was closely correlated to the degree of membrane destabilization, which was consistent with the strong interaction of PAsp(DPT) with the cellular membrane, even at physiological pH. The results of CLSM, hemolysis, and LDH analysis indicate that the membrane-destabilizing capacity of PAsp(DPT) contributes to the intracellular transport of PAsp(DPT) polyplexes, despite its weak buffering capacity. In contrast, the membrane destabilizing capacity of PAsp(DET) was highly altered, depending on the environmental pH. Two cationic charge states emerged with a monoprotonation at neutral pH and a diprotonated state at acidic conditions. We conclude that PAsp(DET) exhibits pH-selective membrane destabilization for late endosomal or lysosomal escape without compromising the membrane integrity of cytoplasmic vesicles and/or organelles. This unique approach provides the impetus for future nonviral gene vector development from synthetic poly(amino acids) with facile insertion of pH-selective membrane destabilizing structures to augment transfection efficacy and limit cytotoxicity. Thus, we show a novel and effective method to construct smart carrier systems useful for intracellular delivery of versatile bioactive components with inherently poor permeability to cellular membranes.

Acknowledgment. This work was financially supported by the Core Research Program for Evolutional Science and Technology (CREST) from the Japan Science and Technology Corp. (JST) as well as by Special Coordination Funds for Promoting Science and Technology from the Ministry of Education, Culture, Sports, Science and Technology of Japan (MEXT). The authors express their appreciation to Dr. H. Hamada (RIKEN, Japan) for providing the plasmid DNA and Dr. Darin Y Furgeson (University of Wisconsin—Madison) for proofreading of the manuscript. K. Miyata thanks the Research Fellowships of the Japan Society for the Promotion of Science for Young Scientists (JSPS) and the Mitsubishi Chemical Corp. Fund for their financial support.

Supporting Information Available: Experimental Section, Supporting Scheme 1, Supporting Figures 1−4, and Supporting Table 1. This material is available free of charge via the Internet at http://pubs.acs.org.

JA804561G

Pharmaceutical Research, Vol. 25, No. 12, December 2008 (© 2008)
DOI: 10.1007/s11095-008-9720-2

Research Paper

Polyplex Micelles from Triblock Copolymers Composed of Tandemly Aligned Segments with Biocompatible, Endosomal Escaping, and DNA-Condensing Functions for Systemic Gene Delivery to Pancreatic Tumor Tissue

Kanjiro Miyata,[1,6] Makoto Oba,[2] Mitsunobu R. Kano,[3,6] Shigeto Fukushima,[4] Yelena Vachutinsky,[1] Muri Han,[5] Hiroyuki Koyama,[2] Kohei Miyazono,[3,6] Nobuhiro Nishiyama,[4,6] and Kazunori Kataoka[1,4,5,6,7]

Received June 26, 2008; accepted August 26, 2008; published online September 10, 2008

Purpose. For systemic gene delivery to pancreatic tumor tissues, we prepared a three-layered polyplex micelle equipped with biocompatibility, efficient endosomal escape, and pDNA condensation functions from three components tandemly aligned; poly(ethylene glycol) (PEG), a poly(aspartamide) derivative with a 1,2-diaminoethane moiety (PAsp(DET)), and poly(L-lysine).

Materials and Methods. The size and *in vitro* transfection efficacy of the polyplex micelles were determined by dynamic light scattering (DLS) and luciferase assay, respectively. The systemic gene delivery with the polyplex micelles was evaluated from enhanced green fluorescence protein (EGFP) expression in the tumor tissues.

Results. The polyplex micelles were approximately 80 nm in size and had one order of magnitude higher *in vitro* transfection efficacy than that of a diblock copolymer as a control. With the aid of transforming growth factor (TGF)-β type I receptor (TβR-I) inhibitor, which enhances accumulation of macromolecular drugs in tumor tissues, the polyplex micelle from the triblock copolymer showed significant EGFP expression in the pancreatic tumor (BxPC3) tissues, mainly in the stromal regions including the vascular endothelial cells and fibroblasts.

Conclusion. The three-layered polyplex micelles were confirmed to be an effective gene delivery system to subcutaneously implanted pancreatic tumor tissues through systemic administration.

KEY WORDS: gene delivery; PEG; polyplex micelle; TGF-β inhibitor; triblock copolymer.

INTRODUCTION

Successful gene delivery through systemic administration is crucial for the gene therapy of various intractable diseases, including cancer. Use of an appropriate gene vector is needed for systemic administration to achieve selective accumulation of the intact gene in target tissues, and subsequently, to reveal effective gene expression with a sufficient therapeutic index. Although major gene vectors in clinical trials are viral-based systems (1), they could have risks of immunogenicity and mutagenicity that would interfere with their practical use in clinics. Synthetic polymer-based vectors (polyplexes) are attractive alternatives of viruses, because of much lower immunogenicity, greater ease of chemical modification and larger-scale preparation (2–4). To attain successful transfection in tumor tissues *via* intravenous administration by polyplex vectors, several important issues as follows should be addressed: (1) high stability to protect the DNA structure in the biological milieu from nuclease attack, (2) minimized non-specific interaction with biological components to exert longevity in the blood circulation, and (3) smooth escape from endosomes to cytoplasm for efficient gene expression inside target cells.

To fulfill such requirements, polyplexes with poly(ethylene glycol) (PEG) palisades (polyplex micelle) have been prepared by several groups including ourselves through the self-assembly of PEG-polycation copolymers with plasmid DNA (pDNA) (4–8). Indeed, polyplex micelles prepared from PEG–poly(L-lysine) block copolymer (PEG–PLys) showed high tolerability in serum media (9), allowing for a prolonged circulation period of intact pDNA in the blood stream, whereas naked pDNA was completely digested within

[1] Department of Bioengineering, Graduate School of Engineering, The University of Tokyo, 7-3-1 Hongo, Bunkyo-ku, Tokyo, 113-8656, Japan.
[2] Department of Clinical Vascular Regeneration, Graduate School of Medicine, The University of Tokyo, 7-3-1 Hongo, Bunkyo-ku, Tokyo, 113-8655, Japan.
[3] Department of Molecular Pathology, Graduate School of Medicine, The University of Tokyo, 7-3-1 Hongo, Bunkyo-ku, Tokyo, 113-8655, Japan.
[4] The Center for Disease Biology and Integrative Medicine, Graduate School of Medicine, The University of Tokyo, 7-3-1 Hongo, Bunkyo-ku, Tokyo, 113-0033, Japan.
[5] Department of Materials Engineering, Graduate School of Engineering, 7-3-1 Hongo, Bunkyo-ku, Tokyo, 113-8656, Japan.
[6] Center for NanoBio Integration, The University of Tokyo, 7-3-1 Hongo, Bunkyo-ku, Tokyo, 113-8656, Japan.
[7] To whom correspondence should be addressed. (e-mail: kataoka@bmw.t.u-tokyo.ac.jp)

0724-8741/08/1200-2924/0

5 min (10). Nevertheless, PLys-based systems have encountered the issue of inefficient transfection activity, because of the lack of endosome escape, involving a "proton sponge effect" caused by amino groups with a low pKa value as typically reported in poly(ethylenimine) (PEI)-based systems (11,12). Worth noting in this regard is our recent finding that polyplexes from a poly(aspartamide) derivative having 1,2-diaminoethane unit as a side chain, poly[*N*-[*N*-(2-aminoethyl)-2-aminoethyl]aspartamide] (PAsp(DET)), revealed highly efficient transfection with minimal cytotoxicity to a variety of cells including primary cells (13–16), probably due to facilitated endosomal escape based on remarkable change in the protonation degree between physiological pH and endosomal acidic pH. Actually, the PEG–PAsp(DET) polyplex micelle succeeded in *in vivo* transfection of a reporter gene (luciferase) to a rabbit's clamped carotid artery *via* intra-arterial injection (17). Also, when the PEG–PAsp(DET) polyplex micelle was incorporated into a calcium phosphate cement scaffold and then applied in a bone defect model to a mouse skull bone, substantial bone formation surrounding the entire lower surface of the implant was induced by the regulated release of the micelles containing a constitutively active form of activin receptor-like kinase 6 (caALK6) and runt-related transcription factor 2 (Runx2) genes from the scaffold (18). The relatively weak affinity of PAsp(DET) segments to pDNA (19) is also an advantage for the smooth release of the incorporated pDNA and subsequent efficient transcription in the cell interior. On the other hand, such weak affinity probably leads to the detachment of PAsp (DET) chains from pDNA in the polyplex micelle through the interaction with biological components during circulation in the blood stream, resulting in a loss of transfection activity. Therefore, strategies to stabilize the structure of the polyplex micelles against PEG–PAsp(DET) are needed for the development of effective systemic administration methods.

The present study was devoted to develop a PEG–PAsp (DET)-based polyplex micelle for systemic use by conjugating a PLys segment as an anchoring moiety to pDNA at the ω-end of the diblock copolymer. For this purpose, a triblock copolymer of poly(ethylene glycol)-poly[*N*-[*N*-(2-aminoethyl)-2-aminoethyl]aspartamide]-poly(L-lysine) (PEG–PAsp (DET)–PLys) was prepared to integrate three functional segments engendering biocompatibility (PEG), efficient endosomal escape (PAsp(DET)), and effective pDNA condensation (PLys), respectively. In this way, three-layered polyplex micelles can be constructed, in which the middle layer, functioning as an endosomal escape element, is sandwiched between an outer layer of biocompatible PEG and an inner layer of PLys/pDNA polyplex (20). The fluorescence measurement with an intercalator into DNA indicated that pDNA mixed with the triblock copolymers was condensed more tightly than in a PEG–PAsp(DET) diblock copolymer and comparably to a PEG–PLys diblock copolymer. Intracellular trafficking of the polyplex micelles with or without the intermediate layer of PAsp(DET) was compared in detail by confocal fluorescence microscopy to reveal the endosomal escape of the micelles with the PAsp(DET) layer. Finally, reporter gene expression in a subcutaneous pancreatic tumor model, representing an intractable solid tumor with thick fibrosis and hypovascularity, demonstrated that the intravenously injected three-layered polyplex micelles effectively penetrated tumor vasculature in combination with transforming growth factor (TGF)-β type I receptor inhibitor (TβR-I) (21).

MATERIALS AND METHODS

Materials

α-Methoxy-ω-amino-poly(ethylene glycol) (Mw 12,000; PEG–NH_2) and β-benzyl-L-aspartate *N*-carboxy-anhydride (BLA–NCA) were obtained from Nippon Oil and Fats Co., Ltd. (Tokyo, Japan). ε-(Benzyloxycarbonyl)-L-lysine *N*-carboxy anhydride (Lys(Z))–NCA was synthesized from ε-(benzyloxycarbonyl)-L-lysine (Wako Pure Chemical Industries, Ltd., Osaka, Japan) by the Fuchs-Farthing method using bis(trichloromethyl) carbonate (triphosgene; Tokyo Kasei Kogyo Co., Ltd., Tokyo, Japan) (22). Diethylenetriamine (DET; bis(2-aminoethyl)amine), *N*,*N*-dimethylformamide (DMF), dichloromethane, benzene, trifluoroacetic acid, *N*-methyl 2-pyrrolidone (NMP), Tris (tris(hydroxymethyl) aminomethane) and HEPES (2-[4-(2-hydroxyethyl)-1-piperazinyl]ethanesulfonic acid) were purchased from Wako Pure Chemical Industries, Ltd., Osaka, Japan. DMF and dichloromethane distilled by conventional methods were used for the polymer synthesis. DET was distilled over CaH_2 under reduced pressure, and then used for the aminolysis reaction. A pDNA coding for luciferase with a CAG promoter provided by RIKEN (Japan) was used after the amplification in competent DH5α *Escherichia coli* and the subsequent purification using a HiSpeed Plasmid MaxiKit purchased from QIAGEN Science Co., Inc. (Germantown, MD, USA). A full-size Label IT Cy5 Labeling Kit was purchased from Mirus Bio Corporation (Madison, WI, USA). Twenty-four- and 96-well culture plates were purchased from Becton Dickinson Labware (Franklin Lakes, NJ, USA). A human hepatocyte, Huh-7, was obtained from the RIKEN Cell Bank (RIKEN Bioresource Center, Japan). A human pancreatic adenocarcinoma cell line, BxPC3, was obtained from the American Type Culture Collection (Manassas, VA, USA). Dulbecco's Modified Eagle's Medium (DMEM) and RPMI medium 1640 were purchased from Sigma-Aldrich Co. (St. Louis, MO, USA). Fetal bovine serum (FBS) was purchased from Dainippon Sumitomo Parma Co., Ltd. (Osaka, Japan). A Luciferase Assay System Kit was purchased from Promega Co. (Madison, WI, USA), and a Micro BCA™ Protein Assay Reagent Kit was purchased from Pierce Co., Inc. (Rockford, IL, USA). TβR-I inhibitor was purchased from Calbiochem (San Diego, CA, USA; LY364947; catalog no. 616451). Rat monoclonal antibody anti-platelet endothelial cell adhesion molecule-1 (PECAM-1), as a marker for vascular endothelial cells, was purchased from BD Pharmingen (Franklin Lakes, NJ, USA), and Alexa647-conjugated secondary antibody to rat IgG was from Invitrogen Molecular Probes (Eugene, OR, USA).

Synthesis of PEG–PBLA–PLys(Z) Triblock Copolymer

A triblock copolymer, PEG–PBLA–PLys(Z), was synthesized as previously described (20). Briefly, the PEG–poly (β-benzyl L-aspartate) diblock copolymer (PEG–PBLA) was synthesized by the ring-opening polymerization of BLA–NCA initiated by PEG–NH_2, followed by the additional ring-

opening polymerization of Lys(Z)-NCA to obtain PEG-PBLA-PLys(Z) (Fig. 1). Different solvents were used for the syntheses of PEG-PBLA with varying degree of polymerization (DP). For example, PEG-PBLA (DP of PBLA=14) was prepared as follows: BLA-NCA (25 eq to the terminal primary amino group of PEG-NH_2) in DMF was added to PEG-NH_2 in DMF under an argon atmosphere, and stirred at 35°C for 20 h. After confirming the end of the polymerization from the disappearance of specific peaks of NCA in the IR spectrum (IR Report-100 spectrometer (JASCO, Tokyo, Japan)), the solution was poured into a mixture of *n*-hexane and ethyl acetate (6:4) to precipitate PEG-PBLA, and the precipitate was filtered and dried *in vacuo*. A series of PEG-PBLA with longer PBLA segments was prepared by a similar protocol with necessary changes in reaction conditions, including molar feed ratios of PEG-NH_2 to BLA-NCA, solvents and reaction times, as summarized in Table I. The obtained PEG-PBLAs were subsequently used for the ring-opening polymerization of Lys(Z)-NCA. Lys(Z)-NCA (50 eq to terminal primary amino group of PEG-PBLA) in a mixture of DMF and dichloromethane was added to PEG-PBLA in dichloromethane (final molar ratio of DMF to dichloromethane=1:10) under an argon atmosphere, and stirred at 35°C for 40 h. After confirming the end of the polymerization as in the case of the polymerization of BLA-NCA, the solution was poured into the 6:4 mixture of *n*-hexane and ethyl acetate to precipitate PEG-PBLA-PLys(Z), and the precipitate was filtered and dried *in vacuo*. Then, acetylation of the amino group of the N-terminal of PEG-PBLA-PLys(Z) was performed using acetic anhydride (3 eq to the terminal amino group of PEG-PBLA-PLys(Z)) in dichloromethane solution.

For estimation of the DP and molecular weight distribution (Mw/Mn) of the obtained PEG-PBLA-PLys(Z), a gel permeation chromatography (GPC) measurement was carried out using a TOSOH HLC-8220 equipped with TSKgel columns (Super AW4000 and Super AW3000X2), and an internal refractive index (RI) detector. NMP with 50 mM LiBr was used as an eluent at a flow rate of 0.3 ml min^{-1} at 40°C.

Preparation of PEG-PAsp(DET)-PLys Triblock Copolymer

Introduction of 1,2-diaminoethane units into the side chain of the PBLA segment in PEG-PBLA-PLys(Z) was performed by aminolysis reaction with excess of DET molecules (13), followed by the deprotection of the Z group with HBr/AcOH (Fig. 1). The typical synthetic procedure of PEG-PAsp(DET)-PLys with DP of PAsp(DET)=36 and PLys=50 was as follows: Three hundred milligram of PEG-PBLA-PLys(Z) (9.2 μmol) was lyophilized from benzene

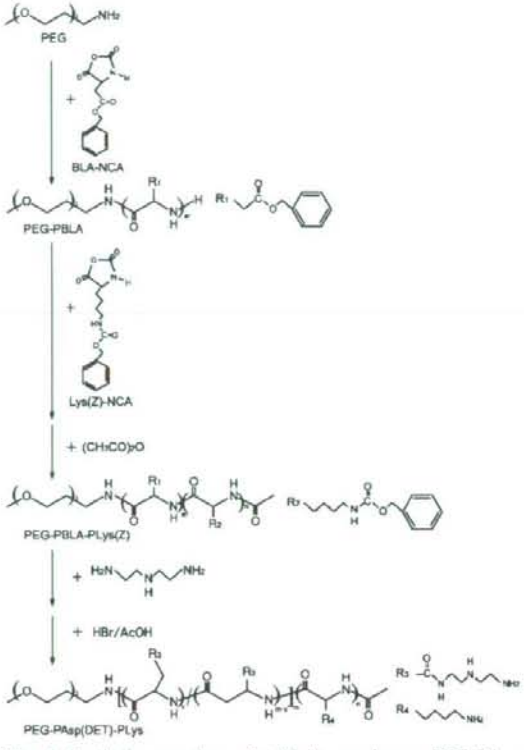

Fig. 1. Synthetic procedure of triblock copolymer, PEG-PAsp (DET)-PLys.

solution and dissolved into 6 mL of DMF. DET (1.8 mL, 16.7 mmol, 50 eq to benzyl groups of PBLA) was added under an argon atmosphere, and stirred at 40°C for 24 h. The mixture was dropped into diethyl ether (80 mL) with stirring, and then the white precipitate was filtered and redissolved in trifluoroacetic acid (2 mL). To deprotect the Z group, HBr (30% in acetic acid) was then added and stirred for 1 h, after which the solution was dropped into diethyl ether (40 mL) with stirring, and the resulting precipitate was purified by filtration and dried *in vacuo*. The crude product was dissolved in distilled water, dialyzed against 0.01 N HCl and then distilled water, and lyophilized to obtain the final product, PEG-PAsp(DET)-PLys as a hydrochloride salt form. The introduction of 1,2-diaminoethane units into the side chain of PAsp and the deprotection of Z group from the PLys(Z) segment were confirmed by ^1H NMR measurement (D_2O,

Table I. Reaction Condition and Composition of PEG-PBLA-PLys(Z)

Code	Molar feed ratio (PEG:BLA:Lys(Z))	Solvent/reaction time (h) for BLA polymerization	Solvent/reaction time (h) for Lys(Z) polymerization	DP of PBLA-PLys (Z)[a]	Mw/Mn[b]
PAsp14(DET)Lys48	1:25:50	DMF/20	DMF+CH_2Cl_2 (1:10)/40	14-48	1.16
PAsp36(DET)Lys50	1:45:50	DMSO/40	DMF+CH_2Cl_2 (1: 10)/40	36-50	1.13
PAsp66(DET)Lys47	1:80:50	DMF + CH_2Cl_2 (1:10)/40	DMF + CH_2Cl_2 (1:10)/40	66-47	1.28

[a] Determined from ^1H NMR.
[b] Determined from GPC.

80°C). In addition, other triblock copolymers, PEG-*b*-poly[*N*-(3-morpholylpropyl)aspartamide]-*b*-PLys (PEG–PAsp(APM)–PLys) and PEG-*b*-poly[*N*-(5-aminopentyl)aspartamide]-*b*-PLys (PEG–PAsp(DAP)–PLys), were similarly prepared by the aminolysis reaction of PEG–PBLA–PLys(Z) with 4-(3-aminopropyl)morpholine (20) and 1,5-diaminopentane (23), respectively. An ^{1}H NMR spectrum was measured with a JEOL EX300 spectrometer (JEOL, Tokyo, Japan). Chemical shifts are reported in ppm downfield from 3-(trimethylsilyl) propionic acid-d_4 sodium salt.

Cytotoxicity of PEG–PAsp(DET)–PLys Triblock Copolymer

A quantitative colorimetric assay with Cell Counting Kit-8 (Dojindo, Kumamoto, Japan) was carried out to evaluate cytotoxicity of block copolymers. This kit utilizes a colorimetric change from a soluble tetrazolium salt (WST-8) to WST-8 formazan by cytosolic dehydrogenases. Huh-7 cells (5,000 cells) were plated on 96-well plates and incubated overnight in 100 μL of DMEM containing 10% FBS. Then, the medium was changed to 100 μL of fresh medium containing 10% FBS and the polymers with various concentrations. After 24 h incubation, the medium was replaced with 100 μL of medium containing 10% FBS without polymers, followed by additional 24 h incubation. The medium was replaced with 120 μL of medium containing 10% FBS and 20 μL of Cell Counting Kit-8 solution, and then, incubated at 37°C for 3 h. The absorbance at 450 nm of the produced WST-8 formazan in each well was measured using a microplate reader (Model 680, Bio-rad). The cytotoxicity of block copolymers was estimated as a growth inhibitory concentration required for 50% reduction in cell population (IC50). The IC50 value of each block copolymer was calculated from a ratio of the obtained absorbance with the polymer to control without polymers. The results are presented as means and standard errors obtained from eight samples.

Preparation of PEG–PAsp(DET)–PLys/pDNA Polyplex Micelle

Each polymer was dissolved in 10 mM Tris–HCl (pH 7.4) buffer at a concentration of 2–5 mg/mL. These polymer solutions were then mixed with pDNA solution in 10 mM Tris–HCl (pH 7.4; final pDNA concentration: 33 μg/mL for *in vitro* assay and 100 μg/mL for *in vivo* assay) at varying mixing ratios.

Ethidium Bromide Exclusion Assay

Each polyplex micelle solution with 33 μg pDNA/mL, prepared by simply mixing pDNA and block copolymers at varying mixing ratios in 10 mM Tris–HCl (pH 7.4), was diluted to 10 μg pDNA/mL containing 2.5 μg EtBr/mL and 150 mM NaCl with the same buffer. The fluorescence intensity of the polyplex micelle solutions at λ=590 nm excited by UV laser (365 nm) was measured using a NanoDrop (ND-3300 Fluorospectrometer, Wilmington, DE, USA). The reference was set with 10 mM Tris–HCl (pH 7.4). The relative fluorescence intensity was calculated as follows:

$$F_r = (F_{sample} - F_0)/(F_{100} - F_0)$$

where F_{sample} is the fluorescence intensity of the micelle samples, F_{100} is that of the free pDNA, and F_0 is the background without pDNA. The results are presented as a mean and standard deviations (SD) obtained from three samples.

Dynamic Light Scattering and Zeta Potential Measurements

DLS and zeta potential measurements were performed using a Zetasizer nanoseries (Malvern Instruments Ltd., UK) at a detection angle of 173° and a temperature of 37°C. An He–Ne laser (λ=633 nm) was used as an incident beam. Polyplex solutions with various N^+/P ratios were prepared to a pDNA concentration of 33 μg/mL in 10 mM Tris–HCl (pH 7.4) buffer. The N^+/P ratio was defined as the molar ratio of protonated amino groups in block copolymers at pH 7.4 to phosphate groups in pDNA. The protonation degrees of lysine and Asp(DET) units at pH 7.4 were estimated to be 1.0 and 0.5, respectively, from the potentiometric titration results (13,24). In the DLS measurement, the sample solutions were injected into a small glass cuvette (volume: 12 μL), ZEN2112 (Malvern Instruments, Ltd.). The data obtained from the rate of decay in the photon correlation function were analyzed by the cumulant method, and the corresponding hydrodynamic diameter of the micelles was then calculated by the Stokes–Einstein equation (25). In the case of zeta potential measurement, the sample solutions were injected into folded capillary cells (Malvern Instruments, Ltd.). From the obtained electrophoretic mobility, the zeta potential was calculated by the Smoluchowski equation:

$$\zeta = 4\pi\eta\upsilon/\varepsilon$$

where η is the viscosity of the solvent, υ is the electrophoretic mobility, and ε is the dielectric constant of the solvent. The results are presented as a mean and SD obtained from three samples.

In Vitro Transfection (Luciferase Assay)

Huh-7 cells (20,000 cells) on 24-well culture plates were incubated with polyplex micelles containing 1 μg pDNA (Lys/Phosphate=2) in 400 μL of DMEM containing 10% FBS, followed by 24-h incubation and replacement with fresh medium. At 24 h post-incubation, the cells were washed with 400 μL of Dulbecco's PBS, and lysed with 200 μL of the cell culture lysis buffer (Promega). The luciferase activity of the lysates was evaluated from the photoluminescence intensity using the Luciferase Assay System and a Mithras LB 940 (Berthold Technologies). The obtained luciferase activity was normalized with the amount of proteins in the lysates determined by the Micro BCA™ Protein Assay Reagent Kit. The results are presented as means and standard errors obtained from four samples.

Cellular Uptake Study of Polyplex Micelles

pDNA was radioactively labeled with ^{32}P-dCTP using the Nick Translation System (Invitrogen, San Diego, CA, USA). Unincorporated nucleotides were removed using High Pure PCR Product Purification Kit (Roche Laboratories, Nutley, NJ, USA). After purification, 2 μg of labeled pDNA

was mixed with 400 μg of non-labeled pDNA. The polyplex micelle samples were prepared by mixing the radioactive pDNA solution with each polymer solution (Lys/Phosphate = 2 and 33 μg pDNA/mL). Huh-7 cells were seeded on 24-well culture plates in DMEM containing 10% FBS. After 24-h incubation, the cells were incubated for 24 h with 30 μL of the radioactive micelle solution (1 μg pDNA/well) in 400 μL of DMEM containing 10% FBS. The cells were then washed three times with Dulbecco's PBS and lysed with 400 μL of the cell culture lysis buffer. The lysates were mixed with 5 mL of scintillation cocktail, Ultima Gold (PerkinElmer, MA, USA), and the radioactivity of the mixtures was measured by a scintillation counter. The results are presented as means and standard errors obtained from four samples.

Intracellular Distribution of Cy5-labeled pDNA Evaluated Through Confocal Laser Scanning Microscope

pDNA was labeled with Cy5 using the Label IT Cy5 Labeling Kit according to the manufacturer's protocol. Huh-7 cells (50,000 cells) were seeded on a 35-mm glass base dish (Iwaki, Japan) and incubated overnight in 1 mL DMEM containing 10% FBS. After replacement of used medium with 1 mL of fresh medium, 90 μL of polyplex solution (Lys/Phosphate=2) containing 3 μg of Cy5-labeled pDNA was applied to the glass dish. After 24-h incubation, the medium was removed and the cells were washed three times with PBS. The intracellular distribution of each polyplex was observed by CLSM after staining acidic late endosomes and lysosomes with LysoTracker Green (Molecular Probes, Eugene, OR, USA) and nuclei with Hoechst 33342 (Dojindo Laboratories, Kumamoto, Japan). The CLSM observation was performed using LSM 510 (Carl Zeiss, Germany) with a ×63 objective lens (C-Apochromat, Carl Zeiss, Germany) at the excitation wavelengths of 488 nm (Ar laser), 633 nm (He–Ne laser), and 710 nm (MaiTai laser for 2-photon imaging) for LysoTracker Green (green), Cy5 (red), and Hoechst 33342 (blue), respectively.

In Vivo Enhanced Green Fluorescence Protein Expression in Subcutaneous Tumor Through Intravenous Injection of Polyplex Micelles

Human pancreatic adenocarcinoma cells (BxPC3) were grown in RPMI medium 1640 supplemented with 10% FBS. BALB/c nude mice (female, 5 weeks old) were obtained from Charles River Laboratories (Tokyo, Japan). All animal experimental protocols were performed in accordance with the Guide for the Care and Use of Laboratory Animals as stated by the NIH. BxPC3 cells (5×10^6 cells in 100 μL of PBS) were injected subcutaneously into the BALB/c nude mice and allowed to grow for 2–3 weeks to reach the proliferative phase. TβR-I inhibitor, dissolved to 5 mg/mL in DMSO and diluted by 100 μL of PBS, was intraperitoneally injected at 1 mg/kg 24 h before polyplex micelle administration. Polyplex micelles (Lys/Phosphate=2) containing EGFP gene in 200 μL of 10 mM HEPES buffer (pH 7.4) were intravenously injected through the tail vein at a dose of 20 μg pDNA/mouse. The mice were sacrificed 3 days after the injection. Tumors were excised, fixed with 10% formalin, and frozen in dry-iced acetone. The frozen samples were further sectioned at a 10-μm thickness in a cryostat. Immunostaining was carried out using anti-PECAM-1 antibody followed by Alexa647-conjugated secondary antibody for staining of vascular endothelial cells. The samples were observed by LSM 510 at excitation wavelengths of 488 and 633 nm for EGFP (green) and Alexa647 (red), respectively.

RESULTS

Preparation of PEG–PAsp(DET)–PLys Triblock Copolymer

A triblock copolymer of PEG, PBLA, and PLys(Z) (PEG–PBLA–PLys(Z)) as a precursor of the cationic triblock copolymer, PEG–PAsp(DET)–PLys, was synthesized by the two-step ring-opening polymerization of BLA–NCA (step 1) and Lys(Z)–NCA (step 2), initiated from the primary amine of PEG–NH_2 as shown in Fig. 1. In this way, a series of triblock copolymers with varying DPs of PBLA and PLys(Z) segments were prepared. As summarized in Table I, the obtained PEG–PBLA–PLys(Z)s were confirmed to have narrow Mw/Mn from the GPC, and the number of repeating units in PBLA and PLys(Z) segments was calculated from the peak intensity ratio of PBLA and PLys(Z) to PEG in the ^{1}H NMR spectra (data not shown). The conversion of flanking benzyl ester in the PBLA segment to *N*-(2-aminoethyl)-2-aminoethyl group was carried out by aminolysis reaction of PEG–PBLA–PLys(Z) with DET, followed by deprotection of the Z group of the PLys(Z) segment to obtain PEG–PAsp (DET)–PLys. The quantitative conversion of PBLA to PAsp (DET) and the complete deprotection of Z group were verified by ^{1}H NMR from the peak intensity ratio of the methylene protons in the *N*-(2-aminoethyl)-2-aminoethyl group ($H_2N(CH_2)_2NH(CH_2)_2NH$–, δ=3.1–3.5 ppm) to the β-methylene protons in the poly(aspartamide) (–$CHCH_2CO$–, δ=2.8 ppm) and the disappearance of the Z group peaks ($C_6H_5CH_2$–, δ=7.3 and 5 ppm), respectively, as typically seen in Fig. 2. The obtained PEG–PAsp(DET)–PLys was abbreviated as PAspX(DET)LysY, where X and Y represent the DP of the PAsp(DET) and PLys segments, respectively. Similarly, control diblock copolymers, PEG–PAsp(DET) and PEG–PLys, were abbreviated as PAspX(DET) and PLysY, respectively.

Cytotoxicity of PEG–PAsp(DET)–PLys Triblock Copolymer

The cytotoxicity of block copolymers, PEG–PAsp(DET), PEG–PLys, and PEG–PAsp(DET)–PLys, was compared and summarized as IC50 values in Table II. Obviously, PEG–PAsp(DET) showed much lower cytotoxicity than the others. The IC50 value of PAsp36(DET)Lys50 at the basis of polymer concentration (μM) was the similar level to that of PLys48, indicating that introduction of PAsp(DET) intermediate segment between PEG and PLys has negligible influence on the cytotoxicity of the block copolymer.

Formation of PEG–PAsp(DET)–PLys/pDNA Polyplex Micelles

Complex formation of pDNA with the triblock copolymer (PAsp36(DET)Lys50) was confirmed by EtBr exclusion assay. While EtBr molecules are known to emit strong fluorescence with their intercalation to DNA duplexes,

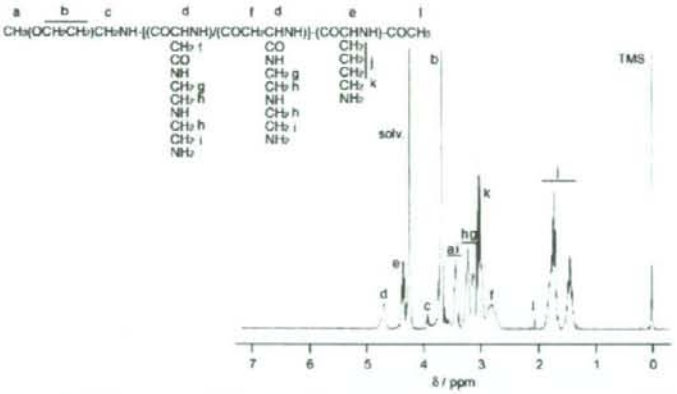

Fig. 2. ^{1}H NMR spectrum of the triblock copolymer, PAsp36(DET)Lys50. (Solvent, D_2O; temperature, 80°C; concentration, 10 mg/mL).

DNA condensation by cationic molecules inhibits such intercalation, resulting in decreased fluorescence. Accordingly, the measurement of the EtBr fluorescence allows the estimation of the process of pDNA condensation (26). The obtained fluorescence data are shown in Fig. 3a. The N/P ratio was defined as the residual molar ratio of total amino groups in the block copolymer to phosphate groups in the pDNA. The fluorescence change in PAsp36(DET)Lys50 seems to reach a plateau at an N/P ratio of 1.5. On the other hand, PLys48 and PAsp39(DET) as control diblock polycations reached plateaus at different N/P ratios; i.e., 1 for PLys48 and 2 for PAsp39(DET). In the plateau region, the fluorescence intensity was similar between PLys48 and PAsp36(DET)Lys50 possessing the PLys segment, while PAsp39(DET) showed higher fluorescence intensity than the others. This result suggests that the PLys segment may have higher ability of pDNA condensation than the PAsp(DET) segment to induce effective dye-exclusion. Then, the fluorescence data was replotted against the residual molar ratio of protonated amino groups to phosphate groups (N^+/P ratio; Fig. 3b). The protonation degree of Lys and Asp(DET) units at pH 7.4 was defined as 1.0 and 0.5, respectively, which were determined from potentiometric titration results of PEG–PLys (24) and PEG–PAsp(DET) diblock copolymers (13). Interestingly, in Fig. 3b, fluorescence profiles of all the samples showed similar trends, leveling off around the N^+/P ratio of 1, indicating that the protonated fraction of amino groups principally participates in the complexation with phosphate groups in the pDNA.

Table II. Growth Inhibitory Effects of the Block Copolymers Against Huh-7 Cells

Sample	IC50		
	Polymer concentration (μg/mL)	Polymer concentration (μM)	Amine concentration (μM)
PAsp68(DET)	>225	>7.35	>1,000
PLys48	26.1±1.4	1.2±0.1	57.0±3.1
PAsp36(DET)Lys50	29.5±0.8	0.9±0.04	114.4±4.9

Size and Zeta Potential of PEG–PAsp(DET)–PLys/pDNA Polyplex Micelles

The size and surface charge of gene vectors crucially affect their biological performance. Thus, these values of the polyplex micelles were determined by DLS and zeta potential measurements, respectively. As shown in Fig. 4a, the size of polyplex micelles gradually decreased with the N^+/P ratio, converging to the range of 60–80 nm in the region of N^+/P>2. The polyplex micelles from the triblock copolymer (PAsp36 (DET)Lys50) were slightly smaller in size than those from the diblock copolymers (PAsp39(DET) and PLys48). As seen in Fig. 4b, all of the polyplex micelles showed almost neutral zeta potential at the N^+/P ratio of 1. Nevertheless, the micelles kept their initial size without any agglomeration even after overnight standing, as is consistent with the formation of a PEG palisade surrounding the polyplex core. Increasing the N^+/P ratio from 1 caused an increase in the zeta potential to a positive value, presumably due to the adsorption of excess block copolymers to the polyplex micelles as previously observed for PEG–P[Lys-*random*-Asp (DET)] block copolymer systems (19). The most prominent increase in the zeta potential with N^+/P was observed for the PAsp36(DET)PLys50 system, which may be explained by the decrease in PEG density of polyplex micelles due to the relative increase in the total length of cationic segments in the block copolymers; e.g., 39 for PAsp39(DET), 48 for PLys48, and 86 for PAsp36(DET)Lys50. Providing the micelles have the same compositional N^+/P ratio at a given feeding N^+/P ratio, the density of PEG should decrease with an increase in the length of the cationic segment. In this regard, the values of the zeta potential were compared between PAsp36(DET) Lys50 triblock micelles and PLys109 diblock (PEG–PLys) micelles having longer-length cationic PLys segments (Fig. 4c). Obviously, the PAsp36(DET)Lys50 micelles still had higher zeta potential than the PLys109 micelles. This finding indicates that the zeta potential of polyplex micelles in the region of excess block copolymers is not simply correlated to the length of the cationic segment, and that the difference in the chemical structure of cationic amino acid residues, in this case Lys and PAsp(DET), crucially affects the composition and structure of the polyplex micelles.

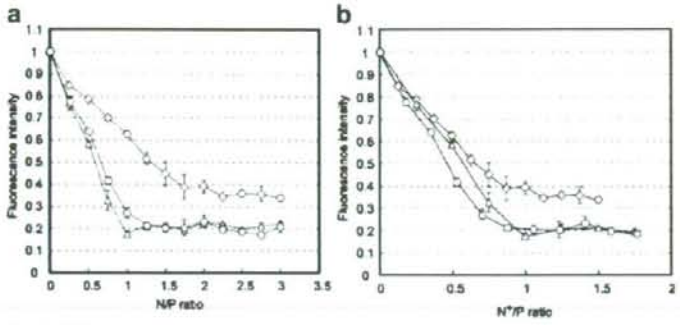

Fig. 3. EtBr dye exclusion assay on the polyplex micelles with varying compositions prepared from PAsp39(DET) (*diamonds*), PLys48 (*triangles*), and PAsp36(DET)Lys50 (*circles*; pDNA concentration, 10 μg/mL; EtBr concentration, 2.5 μg/mL; Temperature, 25°C; Medium, 10 mM Tris–HCl (pH 7.4) containing 150 mM NaCl). **a** The relationship with the N/P ratio, i.e., the residual molar ratio of amino groups in the polymer to phosphate groups in the pDNA. **b** The relationship with the N^+/P ratio, the residual molar ratio of protonated amino groups in the polymer to phosphate groups in pDNA at pH 7.4. Results were expressed as mean±SD (n=3).

To verify the influence of the order of the cationic components in the triblock copolymer, the zeta potential of the polyplex micelles from PEG–PLys–PAsp(DET) (the DPs of PLys and PAsp(DET) were 48 and 33, respectively) was also measured. As seen in Fig. 4d, the polyplex micelles from PLys48Asp33(DET) showed the similar level of zeta potential to those from PLys48. This indicates that PAsp (DET) aligned as an intermediate segment contributes to the higher zeta potential of the PAsp36(DET)Lys50 (Fig. 4b–d).

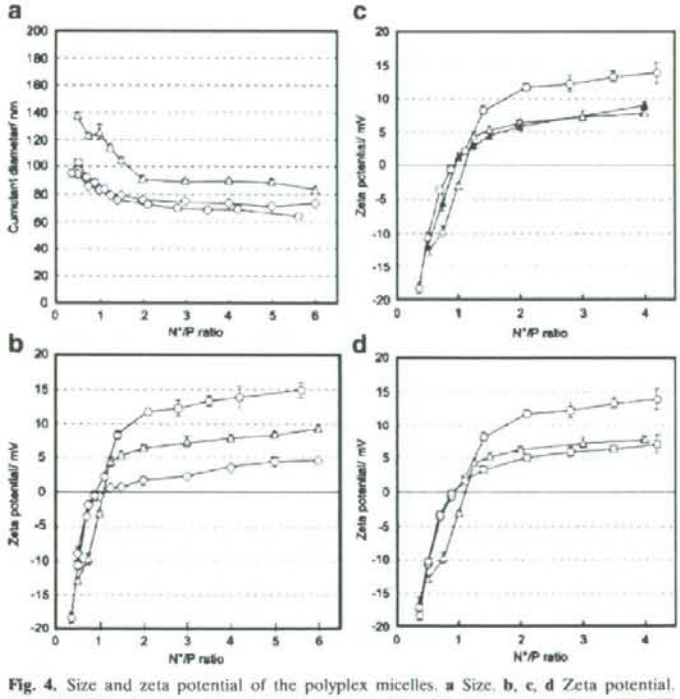

Fig. 4. Size and zeta potential of the polyplex micelles. **a** Size. **b**, **c**, **d** Zeta potential. PAsp39(DET); *diamonds*. PLys48; *empty triangles*. PLys109; *filled triangles*. PAsp36(DET) Lys50; *circles*. PLys48Asp33(DET); *squares*. (pDNA concentration, 33.3 μg/mL; Temperature, 37°C). Results were expressed as mean±SD (n=3).

In Vitro Transfection with Polyplex Micelles Prepared from Triblock Copolymer with Varying Polycations as an Intermediate Segment

Polyplex micelles were prepared from triblock copolymers with different polycation segments aligned between PEG and PLys segments and were subjected to a luciferase assay against Huh-7 cells in order to explore whether the change in the chemical composition of the intermediate polycation layer affects the transfection efficiency. As will be addressed in "DISCUSSION" section, the polyplex micelles from triblock copolymer is likely to take three layered structure at least in the region of excess polycation ($N^+/P>1$): the outer layer of PEG, the middle layer of buffering polycation, and the inner core of condensed PLys/pDNA polyplex (20). PLys segment, which is almost fully charged at physiological pH, is assumed to principally participate in the polyplex formation, keeping the intermediate polycation as free form in the middle layer of the micelles. Thus, it may be reasonable to compare the transfection efficiency of these polyplex micelles from the triblock copolymers with different intermediate segments at the fixed Lys/Phosphate ratio instead of N^+/P ratio, because the latter includes the contribution from the charged amino groups that may not directly participate in the polyplex formation. Here, the Lys/Phosphate ratio is fixed to 2 because the previous study revealed that pDNA condensation is completed at this ratio, exerting the optimal transfection efficiency (26).

The DPs of the intermediate polycations (PAsp(DAP), PAsp(APM), and PAsp(DET) as illustrated in Fig. 5a and the PLys in the triblock copolymers were fixed to 36 and 50, respectively, in this experiment. Fig. 5b clearly shows that the luciferase activity strongly depends on the structure of the intermediate polycation segments in the block copolymers. The polyplex micelles from the PAsp36(DAP)Lys50 showed a similar level of luciferase expression as those from the PLys48, indicating that the introduction of PAsp(DAP) segments with a similar pKa value, 9.9, to PLys had a negligible effect on the transfection efficacy. In line with our previous results (20), the polyplex micelles from the PAsp36(APM)Lys50 revealed some improvements in transfection efficacy compared to the PLys48 micelles. Notably, the highest transfection efficacy was achieved by polyplex micelles from the PAsp36(DET)Lys50, which showed tenfold higher luciferase activity than that from PLys48. On the other hand, the polyplex micelles from PEG–PLys–PAsp(DET) (the DPs of PLys and PAsp(DET) were 48 and 33, respectively), where the order of cationic segments between PAsp(DET) and PLys was inversed in the triblock copolymer, exhibited substantially decreased transfection efficacy compared with those from PAsp36(DET)Lys50.

The effect of the length of the cationic segments on the transfection efficacy was then studied in detail as seen in Fig. 5c. There was observed a critical increase in the transfection efficacy for PEG–PLys systems between the PLys20 and PLys48. It should be noted that one order of magnitude higher transfection was always obtained for the triblock systems compared to the diblock systems having similar total DPs of polycation segments (PLys71 *vs.* PAsp36(DET)Lys50 and PLys109 *vs.* PAsp66(DET)Lys47), supporting the result described in the preceding paragraph that the PAsp(DET) segment aligned as the intermediate segment plays a substantial role in the enhanced transfection.

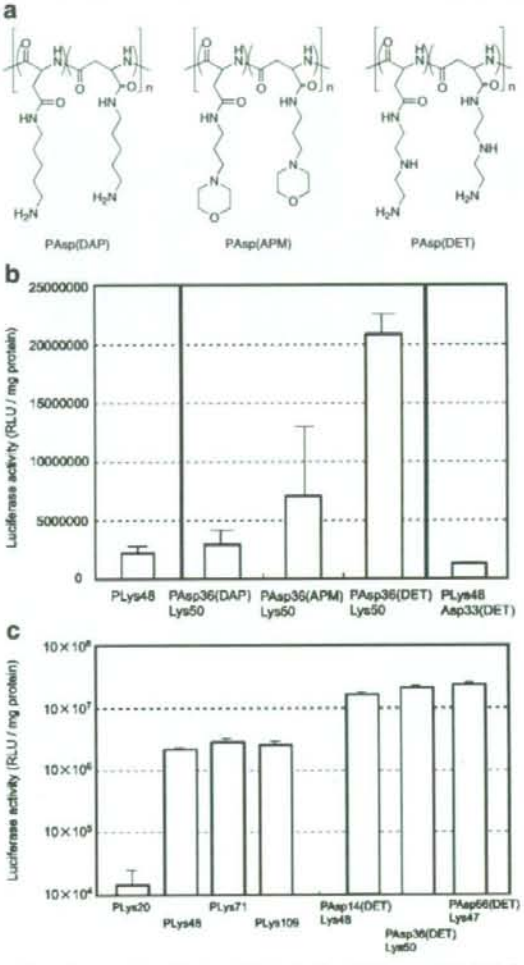

Fig. 5. Transfection efficacy of the polyplex micelles against Huh-7 cells (Luciferase assay). **a** Chemical structures of PAsp(DAP), PAsp (APM), and PAsp(DET) as the intermediate segment in the triblock copolymers. **b** Transfection efficacy of the polyplex micelles from PLys48, a series of triblock copolymers (PAsp36(R)Lys50) with varying intermediate segments (PEG–PAsp(DAP)–PLys, PEG–PAsp(APM)–PLys, and PEG–PAsp(DET)–PLys), and a triblock copolymer with the reversed order of the cationic segments, PLys48Asp33(DET). **c** Effect of the length of the cationic segments in di- or triblock copolymers on transfection efficacy. All the micelle samples were prepared at a Lys/Phosphate= 2 and applied for the transfection (pDNA concentration, 2.3 μg/mL).

Cellular Uptake and Intracellular Distribution of PEG–PAsp (DET)–PLys/pDNA Polyplex Micelles

From the results of luciferase assay, a PAsp(DET) segment integrated into the middle of the triblock copolymers was confirmed to improve the transfection activity of the polyplex micelles, consistent with the hypothesis of facilitated

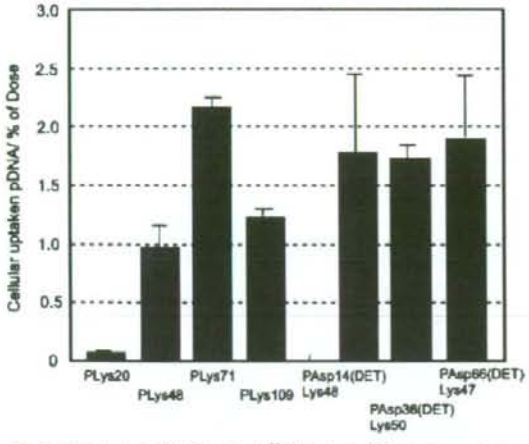

Fig. 6. Uptake into Huh-7 cells of ^{32}P-labeled pDNA in the polyplex micelles. All the micelle samples were prepared at a Lys/Phosphate = 2 and applied for the experiments (pDNA concentration, 2.3 μg/mL).

endosomal escape. Nevertheless, there is also a possibility that the higher zeta potential of PEG–PAsp(DET)–PLys micelles compared to other PEGylated systems (Fig. 4b,c) may facilitate their cellular uptake, leading to the improved transfection. Hence, a cellular uptake study was carried out using ^{32}P-labeled pDNA under a similar condition to the luciferase assay (Fig. 6). PLys20 micelle exhibited significantly lower uptake than those of other micelles, corresponding to its low transfection efficacy as shown in Fig. 5c. All of the micelles prepared from the diblock and triblock copolymers composed of PLys segments with DPs over 47 showed similar levels of cellular uptake. There was no significant difference in the efficacy of cellular uptake between the micelles with and without a PAsp(DET) segment as the middle block, excluding the facilitated cellular uptake as the reason for the improved transfection observed for the polyplex micelles from the triblock copolymers.

Then, intracellular distribution of the polyplex micelles from PLys48 and PAsp36(DET)Lys50 was observed by CLSM to estimate the efficacy of endosomal escape of the polyplex micelles. The pDNA, nuclei, and late endosomes/lysosomes were simultaneously stained with Cy5 (red), Hoechst33342 (blue), and LysoTracker (green), respectively. The Cy5-pDNA introduced into the PLys48 micelles without a PAsp(DET) segment was observed as discrete dots partially colocalizing with the late endosome/lysosome markers (yellow spots) 24 h after the addition of the polyplex micelles (Fig. 7a), indicating that the PLys48 polyplex micelles were segregated in intracellular compartments including late endosomes/lysosomes. In contrast, the Cy5-pDNA in PAsp36(DET)Lys50 polyplex micelles spread more clearly in the cytoplasmic region (Fig. 7b), demonstrating that effective endosomal escape had occurred. These results strongly support that the PAsp(DET) segment plays a crucial role in facilitating the endosomal escape of the polyplex micelles.

In Vivo Transfection by PEG–PAsp(DET)–PLys/pDNA Polyplex Micelle by Intravenous Administration

The transfection ability of the PAsp36(DET)Lys50 polyplex micelles by systemic administration was estimated from EGFP expression in subcutaneously xenografted human pancreatic adenocarcinoma, BxPC3. As previously reported, this tumor tissue has a poorly differentiated histology with a certain number of blood vessels and thick fibrotic tissue in the stroma (21); i.e., closely resembling the histology of certain intractable tumors observed in clinical specimens. The fluorescence microscopy of the sectioned xenografted tumors was obtained with immunostaining of tumor vasculature by PECAM-1 (red), and nuclear counter staining (blue; Fig. 8a). Apparently, the BxPC3 tumors were shown to have wide stromal regions (region S) surrounding nests of tumor cells (region T) and blood vasculature (region V). Fig. 8b shows the image of EGFP expression (green) in the BxPC3 tumor tissue receiving intravenous injection of the PAsp36(DET) Lys50 polyplex micelles incorporating pDNA coding for EGFP. The EGFP expression was evident, yet the intensity was very weak. Worth noting is that TβR-I inhibitor, which has been found to facilitate the accumulation of macromolecular drugs in tumor tissues (21), drastically improved the EGFP expression by the PAsp36(DET)Lys50 polyplex micelles (Fig. 8c). Note that the PAsp36(DET)Lys50 polyplex

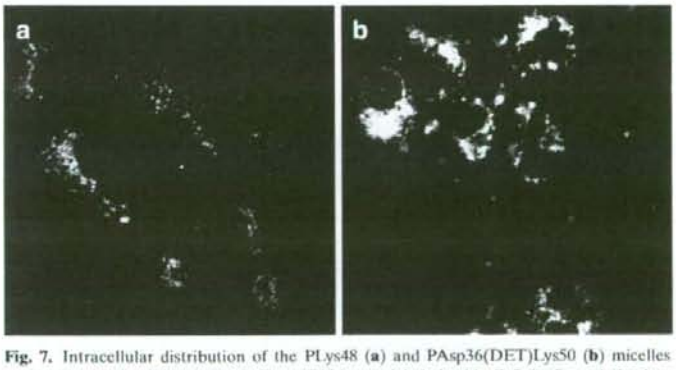

Fig. 7. Intracellular distribution of the PLys48 (**a**) and PAsp36(DET)Lys50 (**b**) micelles prepared at a Lys/Phosphate=2. The pDNA was labeled with Cy5 (*red*), and the late endosomes/lysosomes and the nucleus were stained with LysoTracker (*green*) and Hoechst33342 (*blue*), respectively. (pDNA concentration, 2.8 μg/mL).

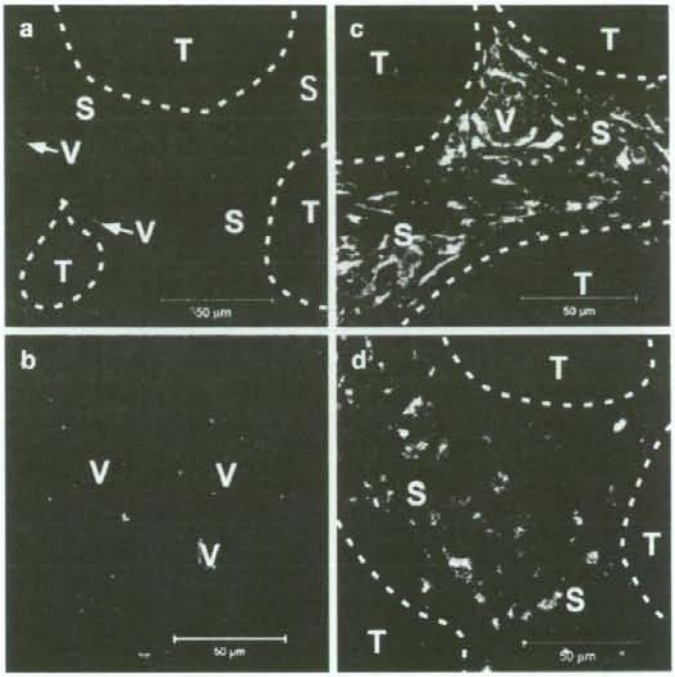

Fig. 8. EGFP transfection into subcutaneous tumors of pancreatic adenocarcinoma cells, BxPC3, *via* systemic route. Each micelle sample was prepared at a Lys/Phosphate=2, and intravenously injected through the tail veins of the mice (20 μg pDNA/mouse). **a** Histology of BxPC3 xenograft as a model of poorly differentiated pancreatic tumor tissue. *Blue*: nucleus stained with Hoechst 33342, *red*: PECAM-1 as an endothelial marker stained with Alexa647-conjugated secondary antibody against anti-PECAM-1 antibody (regions *T*, *S*, and *V* indicate nests of tumor cells in tumor tissues, thick fibrotic tissue in the stroma, and blood vasculature, respectively). **b** EGFP expression by PAsp36(DET)Lys50 polyplex micelle without TβR-I inhibitor; **c** EGFP expression by PAsp36(DET)Lys50 polyplex micelle with TβR-I inhibitor; **d** EGFP expression by PLys71 polyplex micelles with TβR-I inhibitor.

micelles in combination with TβR-I inhibitor did not show detectable EGFP expression in the liver and lung under the tested conditions (data not shown). Fig. 8d shows the result obtained for the PLys71 polyplex micelles with TβR-I inhibitor. Obviously, the EGFP expression by the PAsp36 (DET)Lys50 polyplex micelles was much more remarkable than that with the PLys71 polyplex micelles, suggesting that the integration of the PAsp(DET) segment into the polyplex micelles is effective even in the transfection by systemic administration. Detailed observation of the fluorescence images revealed that the EGFP expression by the polyplex micelles was located mainly around PECAM-1-positive vascular endothelial cells. As typically shown in Fig. 8a, the tumor stroma grows around the nests of tumor cells in BxPC3 subcutaneous xenografts, and blood vasculature exists inside the stroma. Therefore, a major part of the EGFP expression in the BxPC3 tumor by PAsp36(DET)Lys50 polyplex micelles was not from BxPC3 cells *per se*, but from cells in the stroma including vascular endothelial cells and fibroblasts.

DISCUSSION

In the present study, polyplex micelles with an endosomal escape layer were prepared from a triblock copolymer for the purpose of transfection into solid tumors through systemic routes. The triblock copolymer was composed of three tandemly aligned functional segments as follows: PEG for biocompatibility, PAsp(DET) for efficient endosomal escape, and PLys for pDNA condensation. A series of triblock copolymers, PEG–PAsp(DET)–PLys, with the DP of PLys of approximately 50, was synthesized and used for the preparation of the polyplex micelles, according to the previous results that a DP of approximately 48 was needed for effective transfection with polyplex micelles from PEG–PLys as shown in Fig. 5c as well as for the prolonged circulation of intact pDNA in the blood stream (10). The triblock copolymer, PAsp36(DET)Lys50, as well as the diblock PEG–PLys, PLys48, effectively condensed pDNA to form a polyplex micelle (Fig. 3). The obtained polyplex micelles

from the triblock copolymer were around 80 nm at an N^+/P ratio of 1 or greater (Fig. 4a), thereby having the potential ability to accumulate in tumors through the enhanced permeability and retention (EPR) effect (27). Also, the zeta potential measurement indicated that the excess positive charge of the polyplex micelle from the triblock copolymer was reasonably shielded by a PEG palisade surrounding the polyplex core (Fig. 4b). It should be noted that PEGylation of polyplexes facilitates their penetration into tumor spheroids (15, 16). Hence, the PEG palisade of polyplex micelles from the triblock copolymer may contribute to promoting their permeation into the tumor tissue *via* extravasation as well as to extending their plasma half-life through a steric stabilization effect, leading to appreciable gene expression in the subcutaneous pancreatic tumor tissue as seen in Fig. 8. Note that the xenografted pancreatic tumor, BxPC3, was chosen as our target in this study. Since pancreatic tumors are representative of intractable tumors, which are difficult to treat by conventional therapy, they are an appropriate target for the development of new strategies including gene therapy. However, it is also difficult to deliver exogenous genes to such tumor tissue by gene carriers through an EPR effect, presumably due to their thick fibrotic and hypovascular characteristics. In this regard, the combined use of TβR-I inhibitor, which has been found to decrease pericyte coverage of the endothelium specifically in tumor neovasculature (21), is available for the enhancement of accumulation of nano-carriers of 60–100 nm diameter into the solid tumor. Indeed, the EGFP expression by the polyplex micelles from PAsp36(DET)Lys50 was substantially improved by the intraperitoneal injection of TβR-I inhibitor (Fig. 8b,c). The size of the polyplex micelle was approximately 80 nm, thereby making it suitable for combination with TβR-I inhibitor. As far as we know, this is the first example of effective gene expression in BxPC3 tumors with thick fibrotic and hypovascular characteristics *via* systemic administration of non-viral vectors. In addition, detailed observation of the fluorescence images from sectioned xenografted tumors revealed that the EGFP expression by the PAsp36(DET)Lys50 polyplex micelle combined with TβR-I inhibitor was located mainly around the blood vasculature (Fig. 8c), suggesting that the transfection with the polyplex micelle was not effective for the tumor cells *per se*, but for the cells in the tumor stroma, including vascular endothelial cells and fibroblasts. These results suggest that the penetration of polyplex micelles into tumor microenvironments may still be a major challenge, even with the aid of TβR-I inhibitor for successful systemic transfection directly to the BxPC3 tumor cells. In this regard, for the gene therapy of pancreatic adenocarcinoma with thick fibrotic tissues, the approach of treating the tissues surrounding the nests of tumor cells would be more realistic than that directly targeting tumor cells *per se*, e.g., with a tumor suppressor gene to induce apoptosis. Antiangiogenic gene therapy is one of the typical "indirect" approaches to treating fibrotic tumors, and research in this direction on combination treatment using polyplex micelles and TβR-I inhibitor is now ongoing in our laboratory.

The contribution of the PAsp(DET) segment in the triblock copolymer to improved transfection without increased cytotoxicity was obvious from the results of both *in vitro* and *in vivo* transfection studies (Figs. 5, 8, and Table II). It should be noted that there is no significant difference in cellular uptake between the polyplex micelles from the triblock and diblock copolymers (Fig. 6), even though the former revealed almost one order of magnitude higher transfection efficacy than the latter. This result suggests that the major cause for the facilitated transfection with the polyplex micelles from the triblock copolymer may be in the intracellular stage. Indeed, the CLSM observation clearly revealed the facilitated endosomal escape of pDNA associated with the polyplex micelles from the triblock copolymer (Fig. 7), indicating the availability of PAsp(DET) as an endosomal escape element. PAsp(DET) is likely to form the middle layer between the PEG shell and the PLys/pDNA polyplex core in the micelles, because PLys with higher affinity to pDNA than PAsp(DET) is assumed to undergo preferential condensation of pDNA, relegating the PAsp (DET) segment to the boundary with the PEG layer. Increased freedom of PLys as an outer block with a free chain-end may also contribute to the preferential complexation with pDNA. Note that a similar three-layered structure was previously proposed by us for polyplex micelles prepared from PEG–PAsp(APM)–PLys based on the results of ^{1}H-NMR spectroscopy (20). The appreciably higher zeta potential of PAsp36(DET)Lys50 micelles in the region at an N^+/P ratio of 1 or greater is consistent with the formation of a cationic middle layer (Fig. 4b,c) that is not completely shielded by the outer PEG layer. Thus, the PAsp(DET) placed in the middle layer of polyplex micelles should exert endosomal escape ability for efficient transfection through strong buffering and/or a membrane-destabilizing effect based on the unique two-step protonation behavior of the 1,2-diaminoethane unit (13,15). On the other hand, as seen in Fig. 5b, the one order of magnitude lower transfection efficacy obtained by reversing the order of PLys and PAsp (DET) segments in the triblock copolymer is interesting. It is reasonable to consider that arrangement of the PLys segment, with its strong condensing power against pDNA, as the intermediate segment of the triblock copolymer may allow the PAsp(DET) segment to become embedded in the core of the polyplex micelles, resulting in the loss of buffering and/or membrane-destabilizing capacity. The zeta potential of the PEG–PLys–PAsp(DET) systems similar to that of the PEG–PLys systems also supports the disappearance of the intermediate buffering layer in the polyplex micelles from PEG–PLys–PAsp(DET) with the reversed order of the cationic segments (Fig. 4d).

CONCLUSION

For the achievement of systemic gene delivery to solid tumors with appreciable transfection efficacy, gene carriers are required to exert integrated functions including a stealth property in the blood stream to deliver intact pDNA into tumor tissues and permeate target cells with smooth translocation from endosomal compartments into the cytoplasm, subsequently releasing the pDNA to induce effective transcription. In the present study, to develop a gene carrier with such integrated functions, three segments with distinctive functions; i.e., PEG for biocompatibility, PAsp(DET) for endosomal escape, and PLys for pDNA condensation, were tandemly aligned in a polymer strand to form three-layered

polyplex micelles. The obtained micelles showed one order of magnitude higher transfection efficacy against Huh-7, compared to the micelles from the PEG–PLys diblock copolymer without any segments exerting an endosomal escape function. Notably, the polyplex micelle from the triblock copolymer achieved clear *in vivo* transfection of the EGFP gene in fibrotic pancreatic adenocarcinoma, BxPC3, through systemic administration. It should be emphasized that the EGFP expression in the pancreatic tumor was drastically enhanced by the intraperitoneal injection of TβR-I inhibitor prior to the micelle injection, and thus, the potential for combined therapy using polyplex micelles and TβR-I inhibitor for systemic transfection to solid tumors was clearly evidenced. Furthermore, detailed observation of the immunostained tumor tissues revealed that the EGFP expression by the triblock copolymer micelles was located mainly in the stromal tissues surrounding the nests of tumor cells. These results suggest that the triblock micelle is quite promising for fibrotic tumor treatments by the approach of transfecting the tissues surrounding tumor cells, including fibroblasts and endothelial cells, to express proteins inhibiting tumor angiogenesis.

ACKNOWLEDGEMENTS

This work was financially supported by the Core Research Program for Evolutional Science and Technology (CREST) from the Japan Science and Technology Corporation (JST) as well as by Special Coordination Funds for Promoting Science and Technology from the Ministry of Education, Culture, Sports, Science and Technology of Japan (MEXT).

REFERENCES

1. Wiley (2007) Gene Therapy Clinical Trials Worldwide, provided by the *J. Gene Med*. http://www.wiley.co.uk/genetherapy/clinical/ (accessed 17/01/08)
2. D. W. Pack, A. S. Hoffman, S. Pun, and P. S. Stayton. Design and development of polymers for gene delivery. *Nat. Rev. Drug Discov.* **4**:581–593 (2005) doi:10.1038/nrd1775.
3. E. Mastrobattista, M. A. E. M. van der Aa, W. E. Hennink, and D. J. A. Crommelin. Artificial viruses: a nanotechnological approach to gene delivery. *Nat. Rev. Drug Discov.* **5**:115–121 (2006) doi:10.1038/nrd1960.
4. E. Wagner. Strategies to improve DNA polyplexes for *in vivo* gene transfer: Will "artificial viruses" be the answer? *Pharm. Res.* **21**:8–14 (2004) doi:10.1023/B:PHAM.0000012146.04068.56.
5. Y. Kakizawa, and K. Kataoka. Block copolymer micelles for delivery of gene and related compounds. *Adv. Drug Deliv. Rev.* **54**:203–222 (2002) doi:10.1016/S0169-409X(02)00017-0.
6. S. Katayose, and K. Kataoka. Water-soluble polyion complex associates of DNA and poly(ethylene glycol)-poly(L-lysine) block copolymer. *Bioconjugate Chem.* **8**:702–707 (1997) doi:10.1021/bc9701306.
7. M. A. Wolfert, E. H. Schacht, V. Toncheva, K. Ulbrich, O. Nazarova, and L. W. Seymour. Characterization of vectors for gene therapy formed by self-assembly of DNA with synthetic block co-polymers. *Hum. Gene. Ther.* **10**:2123–2133 (1996) doi:10.1089/hum.1996.7.17-2123.
8. Y. H. Choi, F. Liu, J. Kim, Y. K. Choi, J. S. Park, and S. W. Kim. Polyethylene glycol-grafted poly-L-lysine as polymeric gene carrier. *J. Control. Release.* **54**:39–48 (1998) doi:10.1016/S0168-3659(97)00174-0.
9. K. Itaka, A. Harada, K. Nakamura, H. Kawaguchi, and K. Kataoka. Evaluation by fluorescence resonance energy transfer of the stability of nonviral gene delivery vectors under physiological conditions. *Biomacromolecules.* **3**:841–845 (2002) doi:10.1021/bm025527d.
10. M. Harada-Shiba, K. Yamauchi, A. Harada, I. Takamisawa, K. Shimokado, and K. Kataoka. Polyion complex micelles as a vector in gene therapy—pharmacokinetics and *in vivo* gene transfer. *Gene. Ther.* **9**:407–414 (2002) doi:10.1038/sj.gt.3301665.
11. O. Boussif, F. Lezoualc'h, M. A. Zanta, M. D. Mergny, D. Scherman, B. Demeneix, and J. Behr. A versatile vector for gene and oligonucleotide transfer into cells in culture and *in-vivo* polyethylenimine. *Proc. Natl. Acad. Sci. U. S. A.* **92**:7297–7301 (1995) doi:10.1073/pnas.92.16.7297.
12. M. Neu, D. Fischer, and T. Kissel. Recent advances in rational gene transfer vector design based on poly(ethylenimine) and its derivatives. *J. Gene Med.* **7**:992–1009 (2005) doi:10.1002/jgm.773.
13. N. Kanayama, S. Fukushima, N. Nishiyama, K. Itaka, W.-D. Jang, K. Miyata, Y. Yamasaki, U. Chung, and K. Kataoka. A PEG-based biocompatible block catiomer with high buffering capacity for the construction of polyplex micelles showing efficient gene transfer toward primary cells. *Chem. Med. Chem.* **1**:439–444 (2006) doi:10.1002/cmdc.200600008.
14. K. Masago, K. Itaka, N. Nishiyama, U. Chung, and K. Kataoka. Gene delivery with biocompatible cationic polymer: pharmacogenomic analysis on cell bioactivity. *Biomaterials.* **28**:5169–5175 (2007) doi:10.1016/j.biomaterials.2007.07.019.
15. M. Han, Y. Bae, N. Nishiyama, K. Miyata, M. Oba, and K. Kataoka. Transfection study using multicellular tumor spheroids for screening non-viral polymeric gene vectors with low cytotoxicity and high transfection efficiencies. *J. Control Release.* **121**:38–48 (2007a) doi:10.1016/j.jconrel.2007.05.012.
16. M. Han, Y. Bae, N. Nishiyama, and K. Kataoka. Gene delivery with poly(amino acid)-based block catiomer polyplex micelles against multicellular tumor spheroid. *Abstracts of 13th International Symposium on Recent Advances in Drug Delivery Systems*, Salt Lake City, UT, (2007b), pp. 128.
17. D. Akagi, M. Oba, H. Koyama, N. Nishiyama, S. Fukushima, T. Miyata, H. Nagawa, and K. Kataoka. Biocompatible micellar nanovectors achieve efficient gene transfer to vascular lesions without cytotoxicity and thrombus formation. *Gene. Ther.* **14**:1029–1038 (2007) doi:10.1038/sj.gt.3302945.
18. K. Itaka, S. Ohba, K. Miyata, H. Kawaguchi, K. Nakamura, T. Takato, U. Chung, and K. Kataoka. Bone regeneration by regulated *in vivo* gene transfer using biocompatible polyplex nanomicelles. *Mol. Ther.* **15**:1655–1662 (2007) doi:10.1038/sj.mt.6300218.
19. K. Miyata, S. Fukushima, N. Nishiyama, Y. Yamasaki, and K. Kataoka. PEG-based block catiomers possessing DNA anchoring and endosomal escaping functions to form polyplex micelles with improved stability and high transfection efficacy. *J. Control Release.* **122**:252–260 (2007) doi:10.1016/j.jconrel.2007.06.020.
20. S. Fukushima, K. Miyata, N. Nishiyama, N. Kanayama, Y. Yamasaki, and K. Kataoka. PEGylated polyplex micelles from triblock catiomers with spatially ordered layering of condensed pDNA and buffering units for enhanced intracellular gene delivery. *J. Am. Chem. Soc.* **127**:2810–2811 (2005) doi:10.1021/ja0440506.
21. M. R. Kano, Y. Bae, C. Iwata, Y. Morishita, M. Yashiro, M. Oka, T. Fujii, A. Komuro, K. Kiyono, M. Kamiishi, K. Hirakawa, Y. Ouchi, N. Nishiyama, K. Kataoka, and K. Miyazono. Improvement of cancer-targeting therapy, using nanocarriers for intractable solid tumors by inhibition of TGF-beta signaling. *Proc. Natl. Acad. Sci. U. S. A.* **104**:3460–3465 (2007) doi:10.1073/pnas.0611660104.
22. W. H. Daly, and D. Poche. The preparation of *N*-carboxyanhydrides of alpha-amino-acids using bis(trichloromethyl)carbonate. *Tetrahedron Lett.* **29**:5859–5862 (1988) doi:10.1016/S0040-4039(00)82209-1.
23. A. Koide, A. Kishimura, K. Osada, W. -D. Jang, Y. Yamasaki, and K. Kataoka. Semipermeable polymer vesicle (PICsome) self-assembled in aqueous medium from a pair of oppositely charged block copolymers: physiologically stable micro-/nanocontainers of water-soluble macromolecules. *J. Am. Chem. Soc.* **128**:5988–5989 (2006) doi:10.1021/ja057993r.
24. A. Harada, S. Cammas, and K. Kataoka. Stabilized α-helix structure of poly(L-lysine)-block-poly(ethylene glycol) in aque-